NATIONAL ADVISORY COMMITTEE FOR AERONAUTICS

TECHNICAL MEMORANDUM 1314

ON THE TURBULENT FRICTION LAYER FOR RISING PRESSURE

By K. Wieghardt and W. Tillmann

Translation of ZWB Untersuchungen und Mitteilungen
Nr. 6617, November 20, 1944

Washington

October 1951

NATIONAL ADVISORY COMMITTEE FOR AERONAUTICS

TECHNICAL MEMORANDUM 1314

ON THE TURBULENT FRICTION LAYER FOR RISING PRESSURE*

By K. Wieghardt and W. Tillmann

Abstract: As a supplement to the UM report 6603, measurements in turbulent friction layers along a flat plate with rising pressure are further evaluated. The investigation was performed on behalf of the Aerodynamischen Versuchsanstalt Göttingen.

Outline:

1. SYMBOLS

x	position rearward from leading edge of the plate	
y	distance from wall	
u	velocity component in x-direction	
v	velocity component in y-direction	
U,V	velocity components outside of the friction layer	
ρ	density	of the air
μ	viscosity	of the air
ν	kinematic viscosity	of the air
p	static pressure	

*"Zur turbulenten Reibungsschicht bei Druckanstieg." Zentrale für wissenschaftliches Berichtswesen der Luftfahrtforschung des Generalluftzeugmeisters (ZWB), Berlin-Adlershof, Untersuchungen und Mitteilungen Nr. 6617, Kaiser Wilhelm-Institut für Strömungsforschung, Göttingen, November 20, 1944.

$q = \frac{\rho}{2} u^2$ dynamic pressure

$g = p + q$ total pressure

$Q = \frac{\rho}{2} U^2$ dynamic pressure outside of the friction layer

Ux/ν Reynolds number

$U\delta_2/\nu$ Reynolds number of the friction layer

δ friction layer thickness

$\delta_1 = \int_0^\delta \left(1 - \frac{u}{U}\right) dy$ displacement thickness

$\delta_2 = \int_0^\delta \frac{u}{U}\left(1 - \frac{u}{U}\right) dy$ momentum loss thickness

$\delta_3 = \int_0^\delta \frac{u}{U}\left[1 - \left(\frac{u}{U}\right)^2\right] dy$ energy loss thickness

$H_{12} = \delta_1/\delta_2$

$H_{32} = \delta_3/\delta_2$

$\eta = 1 - \left[\frac{u(\delta_2)}{U}\right]^2$

} form parameters of the velocity profile

τ turbulent shearing stress

τ_o wall shearing stress

$c_f' = \tau_o \Big/ \frac{\rho}{2} U^2$ local friction drag coefficient

l mixing length

2. INTRODUCTION

For the calculation of laminar boundary layers in two-dimensional incompressible flow, numerous calculation methods have been developed

on the basis of Prandtl's boundary-layer equation; in contrast, only the semiempirical method of E. Gruschwitz (reference 1) and its improvements by A. Kehl (reference 2) and A. Walz (references 3, 4, and 5) are available for turbulent friction layers. The reason, as is well known, lies in the lack of a mathematical law for the apparent shearing stress τ which originates by the turbulent mixing of momentum. Prandtl's expression for the mixing length so far has led to success only in cases where a sufficient number of correct (and also sufficiently simple) data on the variation of the mixing length can be obtained directly from the geometry of the flow as for instance in the case of the free jet. As a basis for the Gruschwitz method there serve, therefore, besides the momentum equation for friction layers, three statements which are partly empirical and lack a theoretical basis. They are as follows:

A. The velocity profiles in the turbulent friction layer for variable outside pressure form, after having been made adequately dimensionless, a single-parameter family of curves, if one disregards the laminar sublayer; thus, every profile may be characterized by a single quantity (η).

B. A differential equation, likewise derived solely from experiments, concerning the variation of this parameter in flow direction as a function of the pressure variation and of the momentum thickness.

C. An assumption concerning the wall shearing stress. Gruschwitz inserts a constant as first approximation.

A. Kehl (reference 2) then improved the Gruschwitz method. According to his measurements which extended over a larger Re-number range than those of Gruschwitz, it is necessary to insert in statement B, for a higher Re-number of the friction layer, a function of the Re-number $U\delta_2/\nu$ instead of a certain constant b. Furthermore, Kehl obtained better agreement between the calculation and his test results by substituting in statement C for the wall shearing stress the value which results for the respective $\mathrm{Re}(\delta_2)$ number at a flat plate with constant outside pressure. Finally, A. Walz (references 3, 4, and 5) greatly simplified the integration method mathematically so that for prescribed variation of the velocity outside of the friction layer $U(x)$ the momentum thickness, the form parameter η, and hence the point of separation can be calculated very quickly. No statement is obtained regarding the wall shearing stress, since it had, on the contrary, been necessary to make the assumption C concerning τ_0 in order to set up the calculation method at all.

Thus it seemed desirable to investigate the friction drag of a smooth plate for variable outside pressure. On one hand, direct interest in this exists in view of the wing drag; on the other hand, one could

expect an improvement in the above calculation method if an accurate statement regarding τ_o could be substituted for the assumption C. In order to arrive at the simplest possible laws, friction layers along a flat smooth plate were investigated where a systematically increasing pressure was produced by an opposing plate. By analogy with the behavior of laminar boundary layers the wall shearing stress was expected to decrease in the flow direction up until separation, more strongly than in case of constant outside pressure. Instead, τ_o increased, after a certain starting distance, more or less suddenly to a multiple of the initial value. A brief report on this striking behavior of the friction drag has already been published (reference 6). In the present report, these tests are further evaluated and compared with those of Gruschwitz and Kehl. Considerable deviations result in places; however, it was not possible to develop a better calculation method with this new test material either.

Since the application of an energy theorem had proved expedient for the calculation of laminar boundary layers (reference 7), a theoretical attempt in this respect was made for turbulent friction layers, too; however, it did not meet with the same success. Merely an interpretation for the statement B can be obtained in this manner, which is. however, not cogent.

3. TEST SETUP

The test setup and program have been described in the preliminary report. A new measuring method was developed where with the aid of a pressure rake and of a multiple manometer (reference 8) turbulent friction layers could be measured quickly and accurately and the computational evaluation greatly simplified.

Friction layers were measured at $p = 0$ for two different velocities $U = \text{const.}$, four cases, I to IV, with rising, and one, V, with diminishing pressure (figs. 1 to 6). In cases I and II, p increases almost in the entire measuring range linearly with rearward position with respect to the leading edge of the plate x, whereas in cases III and IV the outer velocity U ($U \sim x^{-a}$) decreases with a power of x (figs. 1 to 6).

The velocities were about 20 to 60 meters per second; the test section length was 5 meters so that Re-numbers up to 10^7 were attained. The Re-number of the friction layer (formed with the momentum thickness) increased to from 2 to 7×10^5.

4. TEST RESULTS

Mainly the variation of the wall shearing stress had been described in the brief preliminary report (reference 6); later the measurements were evaluated more thoroughly. First, we plotted figures 1 to 6 for the different pressure variations: the outer velocity U, the local friction drag coefficient c_f', the displacement thickness δ_1, the momentum thickness δ_2, and the energy loss thickness δ_3 treated in section 6; in analogy to the momentum loss thickness δ_2, δ_3 is a measure of how much kinetic energy of the flow is lost mechanically due to the friction layer, that is, is converted to heat by the effect of the friction forces.

In case of constant outside pressure c_f' depends, for a smooth plate, only on the Re-number. The test points from figure 1 lie between the formulas for c_f' according to L. Prandtl (reference 9), F. Schultz-Grunow (reference 10), and J. Nikuradse (reference 11) which in the test range $Ux/\nu = 3 \times 10^5$ to 10^7 differ only slightly. For rising pressure, a slight decrease of c_f' with rearward position results at first, according to figures 2 to 5; however, after a certain distance c_f' increases more or less suddenly to a multiple of its original amount and decreases again only at the end of the test section where for test technical reasons the pressure increase could no longer be maintained. W. Mangler (reference 12) found the same unexpected behavior in further evaluating the measurements of A. Kehl (reference 2). In contrast, c_f' varies only slightly in case of decreasing pressure. Thus, on one hand, $\frac{dp}{dx} > 0$ must be responsible for the strong increase in wall shearing stress; furthermore, the Re-number of the friction layer is of importance since first a certain starting distance is required. Therefore, we plotted in figure 7 c_f' against the dimensionless $\frac{\delta_2}{Q}\frac{dp}{dx}$. Our measurements resulted in a comparatively narrow bundle of curves; however, the results according to Kehl-Mangler, drawn in in dashed lines, cannot be brought under a common denominator in this manner. The test arrangement of Kehl was more general insofar as he had at first a piece of laminar boundary layer and, moreover, in some cases first a pressure drop, and then an adjoining pressure rise; in our tests, in contrast, the friction layer, starting from the leading edge of the plate, had been made turbulent by a trip wire and the pressure increased monotonically.

In want of a better criterion, we can see from figure 7 that the strong increase in friction drag is not to be expected as long as

$$\frac{\delta_2}{Q}\frac{dp}{dx} < 2 \times 10^{-3}$$

The displacement and momentum thickness as well as the wall shearing stress represent only a summary of the development of a friction layer. Therefore, we shall consider below the velocity profiles and shearing stress profiles. The variation of $\frac{u}{U}$ against the rearward position from the leading edge for constant wall distance is particularly illustrative (figs. 8 and 9). In case II (fig. 8), $\frac{u}{U}$ suddenly drops steeply in the layers near the wall whereas it decreases continuously in case IV. Accordingly, the characteristic lengths δ_1, δ_2, and δ_3 increase at these points more strongly than before. Since the drag coefficient c_f' depends essentially on the variation of $\frac{\partial u}{\partial x}$, one recognizes at once in case II the point of maximum wall shearing stress at $x \approx 3.3$ meters.

The shearing stresses are obtained from Prandtl's boundary-layer equation which may be transformed with the aid of the continuity equation and of the Bernoulli equation $\frac{1}{\rho}\frac{dp}{dx} = -UU_x$ valid outside of the friction layer. With $U_x = \frac{dU}{dx}$, $u_x = \frac{\partial u}{\partial x}$, $u_y = \frac{\partial u}{\partial y}$, and $Q = \frac{\rho}{2}U^2$, one obtains

$$\frac{\partial}{\partial y}\frac{\tau}{2Q} = -\frac{U_x}{U} + \frac{u}{U}\frac{u_x}{U} - \frac{u_y}{U}\int_0^y \frac{u_x}{U}\,dy \qquad (1)$$

The integration which is still to be performed yields additionally a control value for the wall shearing stress

$$\frac{\tau_o}{2Q} = \frac{c_f'}{2} = -\int_0^\delta \frac{\partial}{\partial y}\frac{\tau}{2Q}\,dy \qquad (2)$$

However, the value for τ_o obtained in this manner is not as reliable as the one calculated from the momentum theorem because here graphical differentiation is applied more often. According to a suggestion by

Professor Betz, the momentum theorem may be transformed for the calculation of τ_o in the following manner (compare reference 6):

$$\frac{\tau_o}{2Q} = \frac{1}{U^{2+\bar{H}_{12}}} \frac{d}{dx}\left(U^{2+\bar{H}_{12}}\delta_2\right) + \left(H_{12} - \bar{H}_{12}\right)\frac{1}{U}\frac{dU}{dx}\delta_2 \qquad (3)$$

where a suitable mean value of $H_{12} = \delta_1/\delta_2$ is substituted for $\bar{H}_{12}$. Then the second term is small compared to the first and plays only the role of a correction term so that essentially only one graphical differentiation has to be performed.

First, the shearing stress profiles are plotted for constant outside pressure in figure 10. The shearing stress τ with the appertaining wall shearing stress τ_o and the wall distance y with the momentum thickness δ_2 are made dimensionless. These dimensionless profiles are almost completely identical although a systematic variation with the Re-number is recognizable. The profiles τ against y for the two cases II and IV with pressure rise follow in figures 11 and 13; figures 12 and 14 show the corresponding dimensionless shearing stress profiles τ/τ_o against y/δ_2. In the case II where the pressure p increases approximately linearly, the τ-profiles differ considerably for various rearward positions, especially the wall distance at which τ reaches its maximum value is subject to great changes. In contrast, the dimensionless profiles in case IV where $U \approx 53(x/1m)^{-0.27}$ meters per second is valid are very similar. Only the one profile at $X = 1.99$ meters stands out sharply without any perceptible reason. According to D. R. Hartree (reference 13), similar velocity and hence also shearing stress profiles result for laminar boundary layer in the case $U \sim x^{\pm a}$ since for laminar flow τ is simply $\tau = \mu \frac{\partial u}{\partial y}$. In the turbulent friction layer, the velocity and hence also the shearing stress profiles thus vary in this case; however, the latter at least can be described - although somewhat forcibly - by a single-parameter family of curves, according to figure 14.

A. Buri (reference 14) attempted to interpret the shearing stress profiles in general as single-parameter family of curves. Buri selected for the parameter Γ_a the computed wall tangent of the dimensionless shearing stress profile $\Gamma_a = \frac{\delta_2}{\tau_o}\left(\frac{\partial \tau}{\partial y}\right)_{y=0}$ because for this quantity a relation may be read off immediately from the boundary-layer equation.

For $y = 0$, $u = v = 0$ and therewith $\Gamma_a = \frac{\delta_2}{\tau_o}\frac{dp}{dx}$ which yields $\left(\frac{\partial\tau}{\partial y}\right)_{y=0} = \frac{dp}{dx}$. The tangent to the shearing stress profile thus calculated is known in general to fit very badly the shearing stress variation in the proximity of the wall determined from measurements. In the turbulent friction layer, the velocity u decreases only in immediate wall proximity - in the so-called laminar sublayer - to zero so that the tangent direction deviates from the above calculated value even for very small wall distances. This is shown also in figure 15, which represents the shearing stress profiles in wall proximity and the pertaining wall tangents found by calculation; for constant outside pressure, too, the curves against y apparently begin to drop from the point $y = 0$ outward with a definite angle rather than continue with a horizontal tangent (fig. 10). Nevertheless, Γ_a could be used at first as a computed quantity for the characterization of a definite shearing stress profile. However, in case II, for instance, the same shearing stress profile would have to be present for $x = 3.19$ meters and for $x = 3.79$ meters according to figure 15, which is obviously not true according to figure 12. In general, the shearing stress profiles could not be characterized by one other parameter alone either. At least two quantities would be required for this, for instance, the magnitude and the dimensionless wall distance of the maximum τ_{max}/τ_o.

Finally, we calculated from the shearing stress the mixing lengths according to Prandtl's expression $\tau = \rho l^2 \frac{\partial u}{\partial y}\left|\frac{\partial u}{\partial y}\right|$ and plotted them in figures 16 to 19 against the wall distance y or in dimensionless form l/δ_2 against y/δ_2. Like the thickness of the friction layer, l increases more and more with further rearward movement; in case IV, l even increases on approaching the end of the test section to 30 millimeters. The diminishing of the mixing length for large wall distances cannot be specified, as is well known, since l there is computed as the quotient of two small quantities, namely, τ and $\left(\frac{\partial u}{\partial y}\right)^2$. Here again l increases linearly in wall proximity. In the tube, the result had been $l = 0.4y$ and at the plate for constant pressure, according to Schultz-Grunow (reference 10) $l = 0.43y$ (dashed in figs. 17 and 19). Here, at rising pressure, l increases at first again linearly but far more rapidly. In case II, l attains the maximum value $l = 1.1y$ and in case IV even $l = 2.0y$. Although no fixed relation exists between l/y in wall proximity and the wall shearing stress, it is striking in figures 17 and 19 that l/y is largest just for those rearward positions where the wall shearing stress τ_o also (compare figs. 3 and 5) attains its maximum value.

5. ON THE GRUSCHWITZ CALCULATION METHOD

Our test material enables us to examine the basis of the Gruschwitz method enumerated under section 1. The assumption A according to which all turbulent velocity profiles concerned form a single-parameter family of curves is again confirmed in figure 20. Here a few velocity profiles of the different cases I to V are plotted for which the evaluation accidentally had resulted in exactly the same ratio $H_{12} = \delta_1/\delta_2$; the profiles u/U against y/δ_2 with equal H_{12} and hence equal η (compare fig. 27) are in agreement even for different velocities, rearward positions, and pressure variations, thus also after different "previous history." This single-parameter quality covers, however, only the "visible" turbulent part of the profile; the velocities in the laminar sublayer may have a different distribution even for equal η; otherwise, a unique connection would necessarily exist between the wall tangent Γ_a and η or H_{12} which is certainly not the case according to what was said above.

The change of the velocity profiles characterized by the parameters η or H_{12} with change in the rearward position is represented in figures 21 and 22 for all measuring series. The weak but throughout systematic dependence of the profile on the Re-number for constant outside pressure is remarkable; Nikuradse (reference 11), on the other hand, obtained here always the same profile with $\eta = 0.515$ and $H_{12} = 1.302$.

In order to apply the momentum theorem for the Gruschwitz method, the relation between H_{12} and η, necessarily unique for a single-parameter profile class, must be known. The results for all profiles of our measuring series are plotted in figure 23. All of them lie below the curve indicated by Gruschwitz but the majority of Kehl's points also lie below the original Gruschwitz curve. Since, however, all the results do not greatly deviate from one another, the assumption A may be regarded as correct in good approximation. The long dashed curve was calculated by Pretsch (reference 15) for power profiles; the power pertaining to a certain H_{12} is given in the figure at the right. Concerning the short dashed curve, compare section 6.

Matters are different for assumption B. Gruschwitz had obtained from his test evaluation

$$\frac{\delta_2}{Q}\frac{dg(\delta_2)}{dx} = a\eta - b, \text{ with } a = 8.94 \times 10^{-3} \text{ and } b = 4.61 \times 10^{-3}$$

$g(\delta_2)$ is the total pressure at the wall distance δ_2:

$$g(\delta_2) = p + \frac{\rho}{2}\left[u(\delta_2)\right]^2$$

Because of $\eta = 1 - u(\delta_2)^2/U^2$ and the Bernoulli equation outside of the friction layer $p + Q = \text{constant}$, we may also write

$$\frac{dg(\delta_2)}{dx} = \frac{d}{dx}\left[p + Q(1 - \eta)\right] = -\frac{d(Q\eta)}{dx}$$

Kehl, who investigated a larger Re-number range, found b to be additionally dependent on $U\delta_2/\nu$; therefore, he plots

$$b = a\eta - \frac{\delta_2}{Q}\frac{dg(\delta_2)}{dx} = a\eta + \frac{\delta_2}{Q}\frac{d(Q\eta)}{dx} \qquad (4)$$

against $U\delta_2/\nu$. This has been done for our measurements in figure 24. In this diagram, Gruschwitz obtained a horizontal straight line $b = \text{constant} = 4.61 \times 10^{-3}$ and Kehl the plotted curve which, starting from $U\delta_2/\nu = 2 \times 10^3$ slowly drops. These two lines have been drawn solidly as far as measurements existed. Our measurements show that at least for the cases I and II - that is, for linear steep pressure rise - b can be assumed neither as constant nor as a unique function of $U\delta_2/\nu$ since we obtain in this diagram two essentially deviating curves. The same result is obtained also in the cases III and IV for higher Re-numbers. Only for $U\delta_2/\nu < 10^4$, the deviations of the measuring points may be interpreted as scatter. It is not the Kehl relation but the simpler Gruschwitz relation which is confirmed here. For $U\delta_2/\nu < 2 \times 10^3$ Kehl took the drawn variation of b in order to obtain significant calculation results directly behind the transition point from laminar to turbulent flow. The two points with $U\delta_2/\nu < 10^3$ in the case V are not an argument against this b-variation for the reason that the friction layer had been made artifically turbulent to start with by means of the trip wire. Below, we shall attempt a theoretical interpretation of the relation B which so far has been set up and investigated in a purely empirical manner.

Since the variation of the wall shearing stress proved to be very complicated, according to figures 2 to 6, we cannot improve upon assumption C which refers to the wall shearing stress. In order to estimate the effect of this assumption on the calculation, the cases II and IV were calculated with the aid of Walz's simplified integration method under different assumptions regarding c_f'. Figure 25 shows the result for the momentum thickness δ_2. In the momentum theorem, we may put H_{12} = constant since it appears only in one term $2 + H_{12}$ so that even great variations of H_{12} are of relatively small importance. In case II, one obtains better agreement (at least up to $x = 3m$) between calculation and tests by using the expression for c_f' obtained as a function of $U\delta_2/\nu$ for the plate without pressure rise than by putting c_f' = constant. Conversely, the agreement for case IV is better with the assumption c_f' = constant. In view of the actual variation of c_f' which varies from case to case, no generally valid rule can therefore be set up for it, even before the region of the steep rise of c_f'.

The results of the η calculation are represented in figure 26. The three different calculation methods worked out by Walz are based on the following assumptions:

Gruschwitz-Walz b = constant = 4.61×10^{-3}

and

c_f' = constant = 4×10^{-3}

Gruschwitz-Walz b = constant = 4.61×10^{-3}

and

$c_f' = 0.0251(U\delta_2/\nu)^{-1/4}$

Gruschwitz-Kehl-Walz $b = \dfrac{0.0164}{\log\,(U\delta_2/\nu)} - \dfrac{0.85}{U\delta_2/\nu - 300}$

and

$c_f' = 0.0251(U\delta_2/\nu)^{-1/4}$

As was to be expected according to figure 24, the last, most complicated method is precisely the one that shows the greatest deviations compared to the experiment. In our cases II and IV, the first and simplest calculation method is the best. The agreement between that calculation and the test is still good even in the region of steep rise c_f'. From there on, however, large differences result.

6. ON AN ENERGY THEOREM FOR FRICTION LAYERS

Like the approximation methods for laminar boundary layers, the Gruschwitz method is based on Kármán's momentum equation which is obtained by integration of Prandtl's boundary-layer equation with respect to the wall distance y. One obtains thereby a statement on the total momentum loss of the friction layer. In analogy, a statement on the total energy loss in the friction layer caused by the friction can be obtained if the boundary-layer equation

$$\rho u u_x + \rho v u_y = -p_x + \tau_y = \rho U U_x + \tau_y \tag{5}$$

(after addition of $\frac{\rho u}{2}(u_x + v_y) = 0$ because of continuity) is first multiplied by u and then integrated with respect to y

$$-\frac{d}{dx}\int_0^\delta \rho u\left(\frac{1}{2}U^2 - \frac{1}{2}u^2\right) dy + \left[\frac{\rho u^2 v}{2}\right]_0^\delta + \rho\frac{U^2}{2}\int_0^\delta u_x\, dy = \int_0^\delta u\tau_y\, dy$$

and because of $\left[\frac{\rho u^2 v}{2}\right]_0^\delta = \frac{\rho}{2}U^2 V = -\frac{\rho}{2}U^2\int_0^\delta u_x\, dy$

$$-\int_0^\delta u\tau_y\, dy = \int_0^\delta \tau u_y\, dy = \frac{d}{dx}\int_0^\delta \rho u\left(\frac{1}{2}U^2 - \frac{1}{2}u^2\right) dy \tag{6}$$

This equation signifies that the loss in kinetic energy per unit length transverse to the flow direction in the friction layer equals the rate of doing work of the turbulent shearing stresses.

For the laminar boundary layer $\tau = \mu u_y$ is valid so that $\int_0^\delta \tau u_y \, dy = \mu \int_0^\delta u_y^2 \, dy$ here signifies the dissipation, that is, the energy converted to heat per unit time.

In turbulent friction layers, in contrast, no simple relation between the shearing stress and the velocity profile exists; if it did, the essentially single-parameter family of turbulent velocity profiles would have to include also a single-parameter profile class of the shearing stresses which is not the case according to the test evaluation. If we define, corresponding to the momentum loss thickness, an energy loss thickness

$$\delta_3 = \int_0^\delta \frac{u}{U}\left(1 - \left(\frac{u}{U}\right)^2\right) dy \tag{7}$$

and the following dimensionless

$$e = \frac{\text{work of the shearing stresses}}{\text{work against the wall shearing stress}} = \int_0^\delta \frac{\tau}{\tau_o} \frac{\partial}{\partial y} \frac{u}{U} \, dy \tag{8}$$

we can write equation (6) also as

$$e = \frac{1}{c_f' U^3} \frac{d}{dx}\left(U^3 \delta_3\right) \tag{9}$$

Since we have thus obtained one new equation with two new unknowns, this energy theorem at first does not help us any further either. However, we can calculate the energy loss thickness δ_3 from the velocity distributions and obtain, due to the single-parameter quality of the velocity profiles, a fixed relation between the quantities δ_1, δ_2, and δ_3. Plotting thus the ratio $H_{32} = \delta_3/\delta_2$ against $H_{12} = \delta_1/\delta_2$ for all profiles measured, we obtain figure 27. All points come to lie, with only very small deviations, on one "street." For power profiles $u/U = (y/\delta)^n$ the long dashed curve

$$H_{32} = \frac{AH_{12}}{H_{12} - B} \tag{10}$$

would result with $A = 4/3$ and $B = 1/3$. A good fairing curve for the actual profiles at pressure rise and drop results if we put $A = 1.269$ and $B = 0.379$. On the basis of this empirical relation, δ_3 may now be calculated from δ_1 and δ_2 with sufficient accuracy.

If one more relation could be found for the ratio e as well, it would be possible to calculate from the new equation (9) for instance c_f'. The calculation of e from the measuring results is made difficult by the fact that it results as the quotient of two quantities which can both be found only by graphic differentiation. This explains the great variation of the e-values plotted for the different cases in figure 28. On the whole, e varies only comparatively little; even when c_f' for instance in case IV increases from 3 to 16×10^{-3}, e remains between 0.8 and 1.2. At first glance, e seems to have, according to the defining equation (8), the significance of an efficiency which could not exceed 1. Actually, however, e may assume any arbitrary value, according to the velocity and shearing stress profile concerned; in the immediate proximity of turbulent separation, above all, where τ_o vanishes, e may assume arbitrary magnitude.

Because of the inaccuracy of the calculation from the test data, it was not possible to determine for e a relation to the other boundary-layer quantities. However, one can set up an interesting analogy between the energy equation and Gruschwitz's assumption B. If one substitutes the above relation for H_{32} which was found experimentally in the energy equation and eliminates $\frac{d\delta_2}{dx}$ with the aid of the momentum theorem, one obtains

$$\frac{U_x}{U} + \frac{B}{H_{12}(H_{12} - B)(H_{12} - 1)} \frac{dH_{12}}{dx} = \frac{H_{12}(A - 2e) + 2eB}{2AH_{12}(H_{12} - 1)} c_f' \qquad (11)$$

On the other hand, one may differentiate out the Gruschwitz-Kehl relation (assumption B), equation (4), and write

$$\frac{U_x}{U} + \frac{1}{2\eta} \frac{d\eta}{dH_{12}} \frac{dH_{12}}{dx} = \frac{b - a\eta}{2\eta} \qquad (12)$$

regarding η as a function of H_{12}: $\eta = \eta(H_{12})$. We now assume that the relation B follows from the energy theorem. If this is the case,

the left sides of equations (11) and (12) must, first of all, be identical. We therefore equate, as an experiment, the left sides of the equations and obtain a differential equation for $\eta(H_{12})$, the solution of which reads

$$\eta = \text{number} \times H_{12}^{2} \frac{(H_{12} - 1)^{2B/(1 - B)}}{(H_{12} - B)^{2/(1 - B)}} \tag{13}$$

From the $H_{32} - H_{12}$ relation, we had found for B: $B = 0.379$. If, furthermore, we put, for adaptation to the test results, the number equal to 0.986, the function $H_{12}(\eta)$ is, according to figure 23, quite well satisfied by equation (13).

Thus, the left sides of the energy equation (11) and of the relation B (equation (12)) seem to be identical. Then the right sides also must be equal which - solved with respect to b - results in

$$b = a\eta + \frac{H_{12}(A - 2e) + 2eB}{AH_{12}(H_{12} - 1)} c_f'\eta \quad \text{with} \quad A = 1.269 \quad \text{and} \quad B = 0.379 \tag{14}$$

Therewith, a relation between quantities of the velocity and of the shearing stress profile, based on the energy theorem, has been found for the assumption of the Gruschwitz method. In practice, of course, this equation is of no help, either, since no data concerning the newly introduced quantity e are available although one deals here, according to the defining equation (8), with a comparatively illustrative quantity. Thus one may conclude from equation (14) only that it is improbable that invariably b = constant (as Gruschwitz assumes) or that b depends solely on $U\delta_2/\nu$ (as Kehl presupposes), for b appears here as a function of the respective velocity profile (η and H_{12}) as well as of e and c_f' which likewise is not determined merely by $U\delta_2/\nu$. However, theoretically this conclusion is not cogent, either. It is, in itself, conceivable that the course of the turbulence mechanism is such that, in spite of different previous history, the complicated relations between η, c_f', and e have precisely the properties which cause b to be, for every rearward position, for instance a function of $U\delta_2/\nu$ only and the test evaluation according to figure 24 actually shows that b, at least within a certain region, hardly varies.

7. SUMMARY

The report deals with measurements in the turbulent friction layer along a flat plate where the static pressure from the leading edge of the plate onward systematically rises or decreases. In case of pressure rise, there results after a certain starting distance, a large increase in wall shearing stress to a multiple of the initial value; this has already been briefly commented on in the report UM Nr. 6603. The further evaluation of the test material (calculations of the shearing stresses and mixing lengths) also gave qualitative information on this problem. As rule of thumb, it can merely be said that this strong increase in friction drag does not occur as $\frac{\delta_2}{Q}\frac{dp}{dx} < 2 \times 10^3$ is valid.

Furthermore, the empirical relations on which the Gruschwitz method is based are checked with the aid of the measurements. It is again confirmed that the turbulent velocity profiles form with sufficient accuracy a single-parameter family. Gruschwitz obtains from an empirical relation a differential equation for the variation of that parameter in flow direction; Kehl improved that equation by not fixing a quantity b contained in it as constant, like Gruschwitz, but by considering it as a function of the Re-number of the friction layer. The present measurements confirm at first the simple relation b = constant. However, for higher Re-numbers of the friction layer - in the region of strongly increasing wall shearing stresses - different values for b result, according to the previous history of the friction layer; here a relation of the form $b = b(U\delta_2/\nu)$ is no longer sufficient, either. It is shown that this Gruschwitz-Kehl relation can be interpreted as statement of the energy theorem applied to friction layers. However, this energy theorem which simply signifies that the work of the turbulent shearing stresses equals the loss of kinetic energy in the friction layer does not provide any practical help (for instance for setting up a calculation method). As long as a sufficient statement for calculation of the shearing stresses themselves is lacking, a link between the newly introduced total work of the shearing stresses and the known friction layer quantities, $\frac{dp}{dx}$ displacement or momentum thickness, etc., also is lacking. For the same reason, it is not even possible to calculate the wall shearing stress; an approximation value for it must be inserted in the Gruschwitz method. Thus the result of the present investigation is,

on the whole, negative with respect to the problem of calculating in advance turbulent friction layers; however, the test material represented in the figures might prove useful for further theoretical considerations.

Translated by Mary L. Mahler
National Advisory Committee
for Aeronautics

8. REFERENCES

1. Gruschwitz, E.: Die turbulente Reibungsschicht in ebener Strömung bei Druckabfall und Druckanstieg. Ing.-Archiv, Bd. II, Heft 3, September 1931, pp. 321-346.

2. Kehl, A.: Untersuchungen über konvergente und divergente, turbulente Reibungsschichten. Ing.-Archiv, Bd. XIII, Heft 5, 1943, pp. 293-329. (Available as R.T.P. Translation No. 2035, British Ministry of Aircraft Production.)

3. Walz, A.: Graphische Hilfsmittel zur Berechnung der laminaren und turbulenten Reibungsschicht. Lilienthal-Gesellschaft für Luftfahrtforschung Bericht S 10, 1940, pp. 45-74.

4. Walz, A.: Zur theoretischen Berechnung des Höchstauftriebsbeiwertes von Tragflügelprofilen ohne und mit Auftriebsklappen. ZWB Forschungsbericht Nr. 1769, March 1943.

5. Walz, A.: Näherungsverfahren zur Berechnung der laminaren und turbulenten Reibungsschicht. Untersuchungen und Mitteilungen Nr. 3060.

6. Wieghardt, K.: Ueber die Wandschubspannung in turbulenten Reibungsschichten bei veränderlichem Aussendruck. Untersuchungen und Mitteilungen Nr. 6603.

7. Wieghardt, K.: Ueber einen Energiesatz zur Berechnung laminarer Grenzschichten. (Available from CADO, Wright-Patterson Air Force Base, as ATI 33090.)

8. Wieghardt, K.: Staurechen und Vielfachmanometer für Messungen in Reibungsschichten. Technische Bericht, Bd. 11, No. 7, 1944, p. 207.

9. Prandtl, L.: Zur turbulenten Strömung in Rohren und längs Platten. AVA-Ergebn. IV. Lief., 1932, p. 18.

10. Schultz-Grunow, F.: Neues Reibungswiderstandsgesetz für glatte Platten. Luftfahrtforschung, Vol. 17, No. 8, Aug. 20, 1940, p. 239. (Available as NACA TM 986.)

11. Nikuradse, J.: Turbulente Reibungsschichten. Publication of the ZWB, 1942.

12. Mangler, W.: Das Verhalten der Wandschubspannung in turbulenten Reibungsschichten mit Druckanstieg. Untersuchungen und Mitteilungen Nr. 3052, 1943.

13. Hartree, D. R.: On an Equation Occurring in Falkner and Skan's Approximate Treatment of the Equations of the Boundary Layer. Proc. Cambridge Phil. Soc., vol. 33, pt. 2, April 1937, pp. 223-239.

14. Buri, A.: Eine Berechnungsgrundlage für die turbulente Grenzschicht bei beschleunigter und verzögerter Grundströmung. Eidgenössische Technische Hochschule, Zürich, 1931. (Available as R.T.P. Translation No. 2073, British Ministry of Aircraft Production.)

15. Pretsch, J.: Zur theoretischen Berechnung des Profilwiderstandes. Jahrbuch 1938 der deutschen Luftfahrtforschung, p. I 60. (Available as NACA TM 1009.)

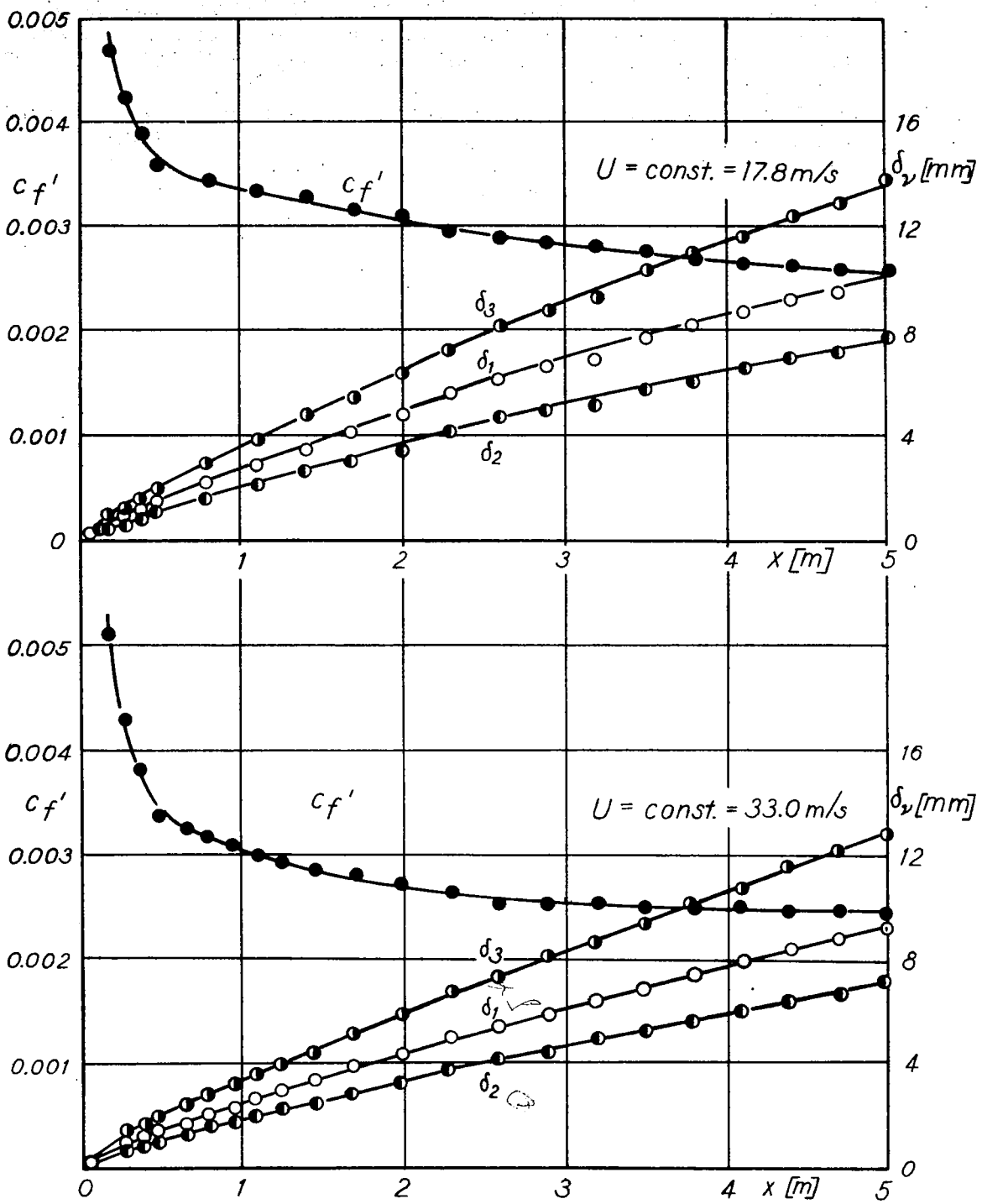

Figure 1.- Constant outer velocity, displacement, momentum, and energy thickness; local drag coefficient.

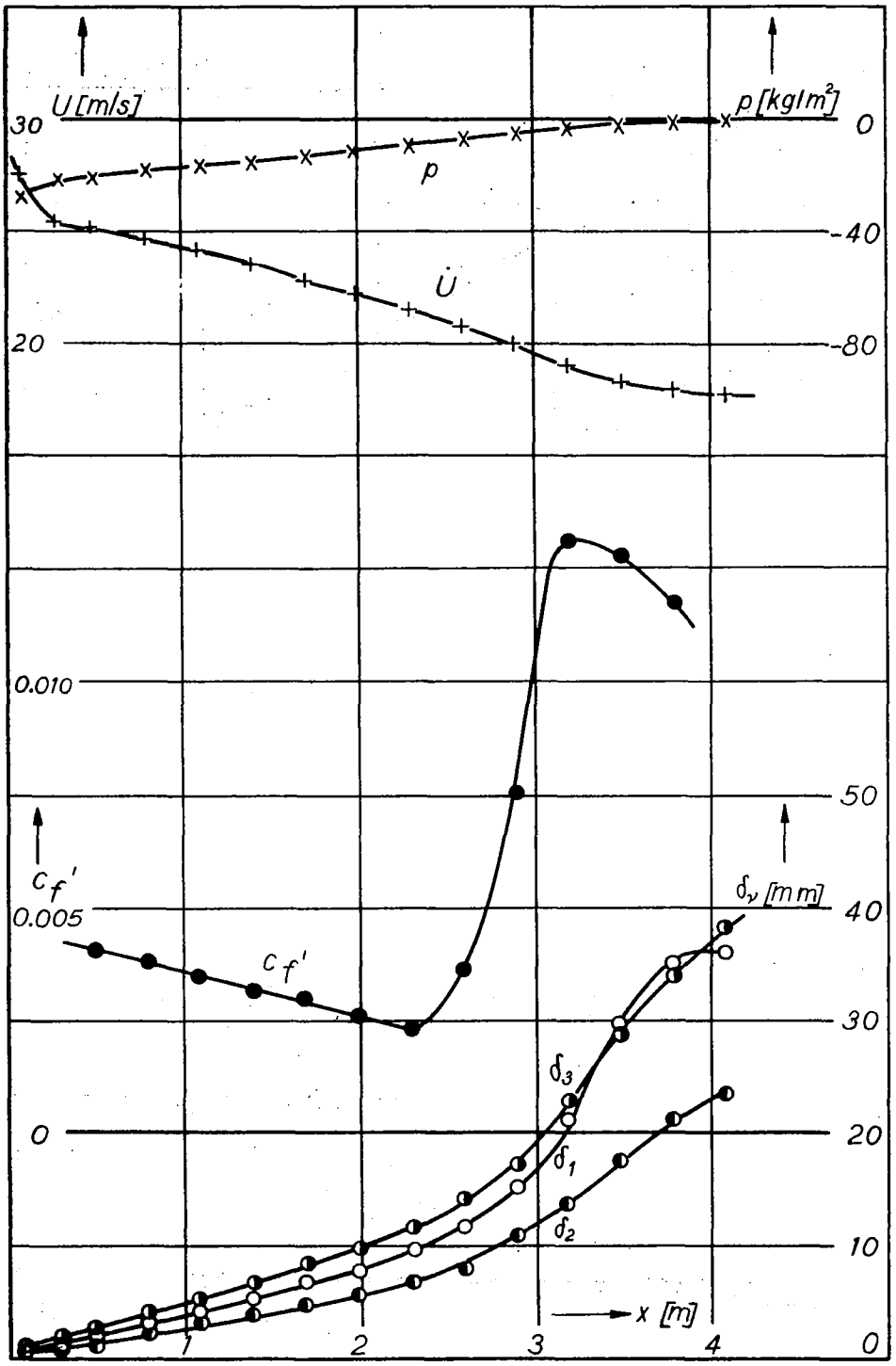

Figure 2.- Pressure rise: Case I. Displacement, momentum, and energy thickness; local drag coefficient.

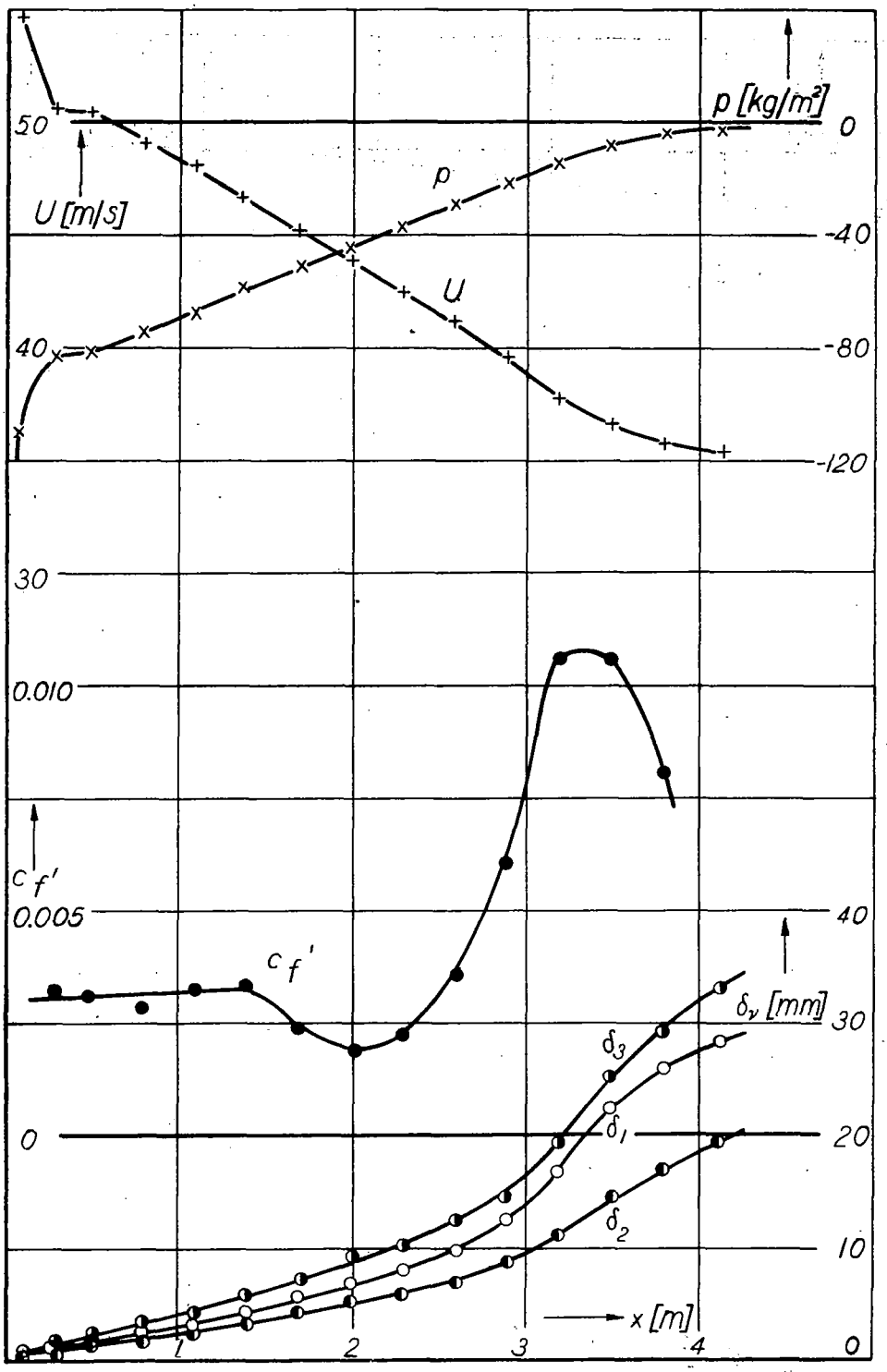

Figure 3.- Pressure rise: Case II. Displacement, momentum, and energy thickness; local drag coefficient.

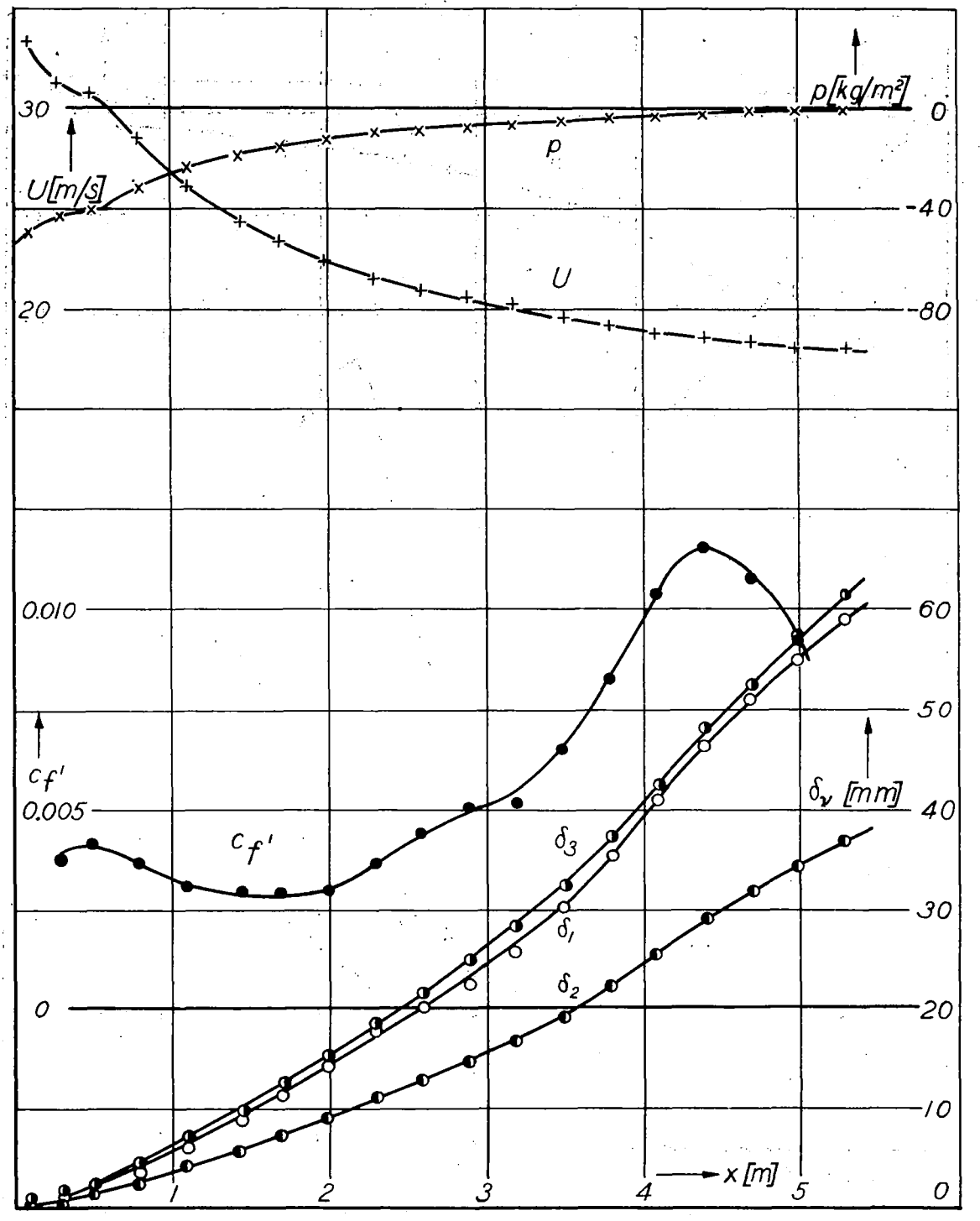

Figure 4.- Pressure rise: Case III. Displacement, momentum, and energy thickness; local drag coefficient.

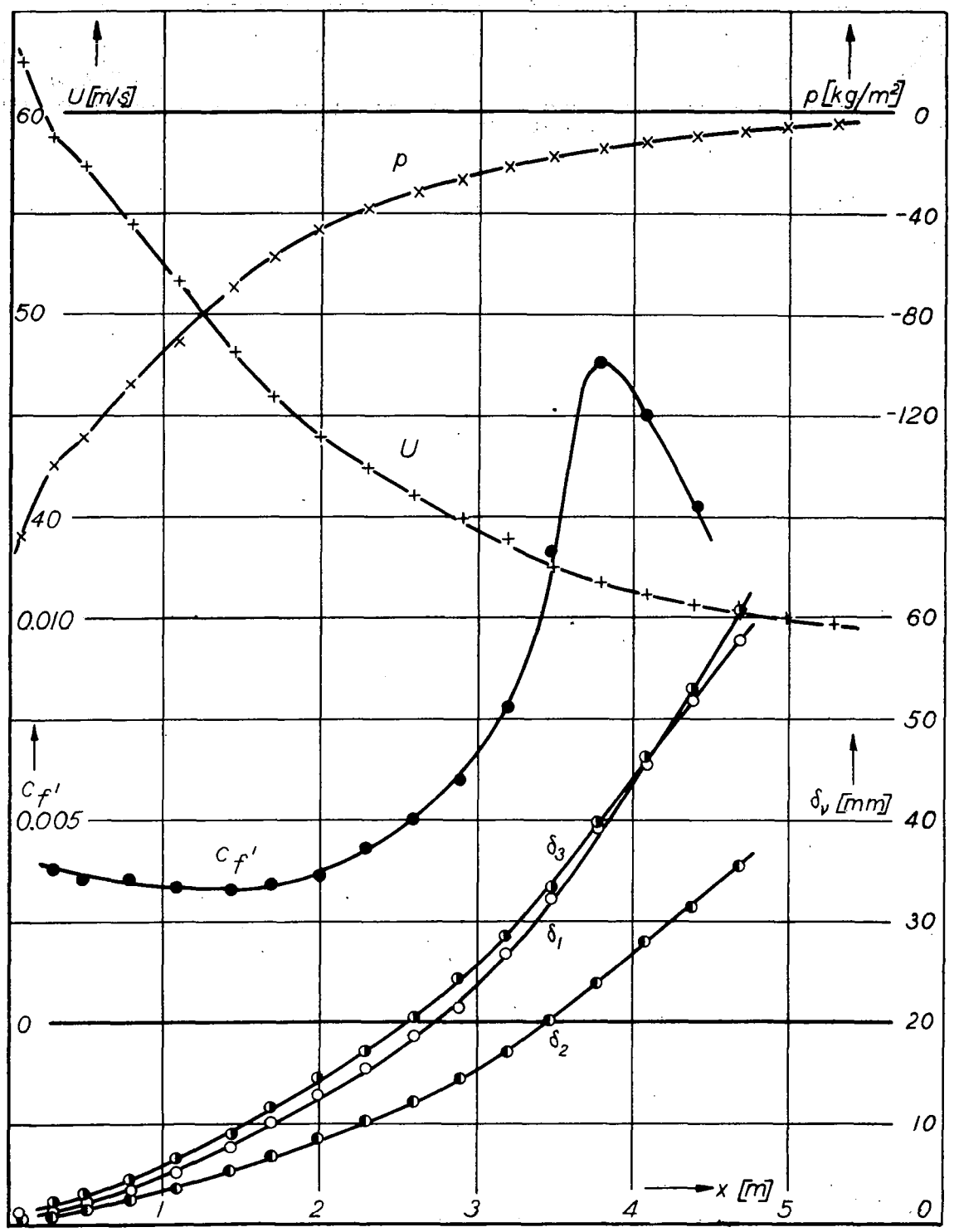

Figure 5.- Pressure rise: Case IV. Displacement, momentum, and energy thickness; local drag coefficient.

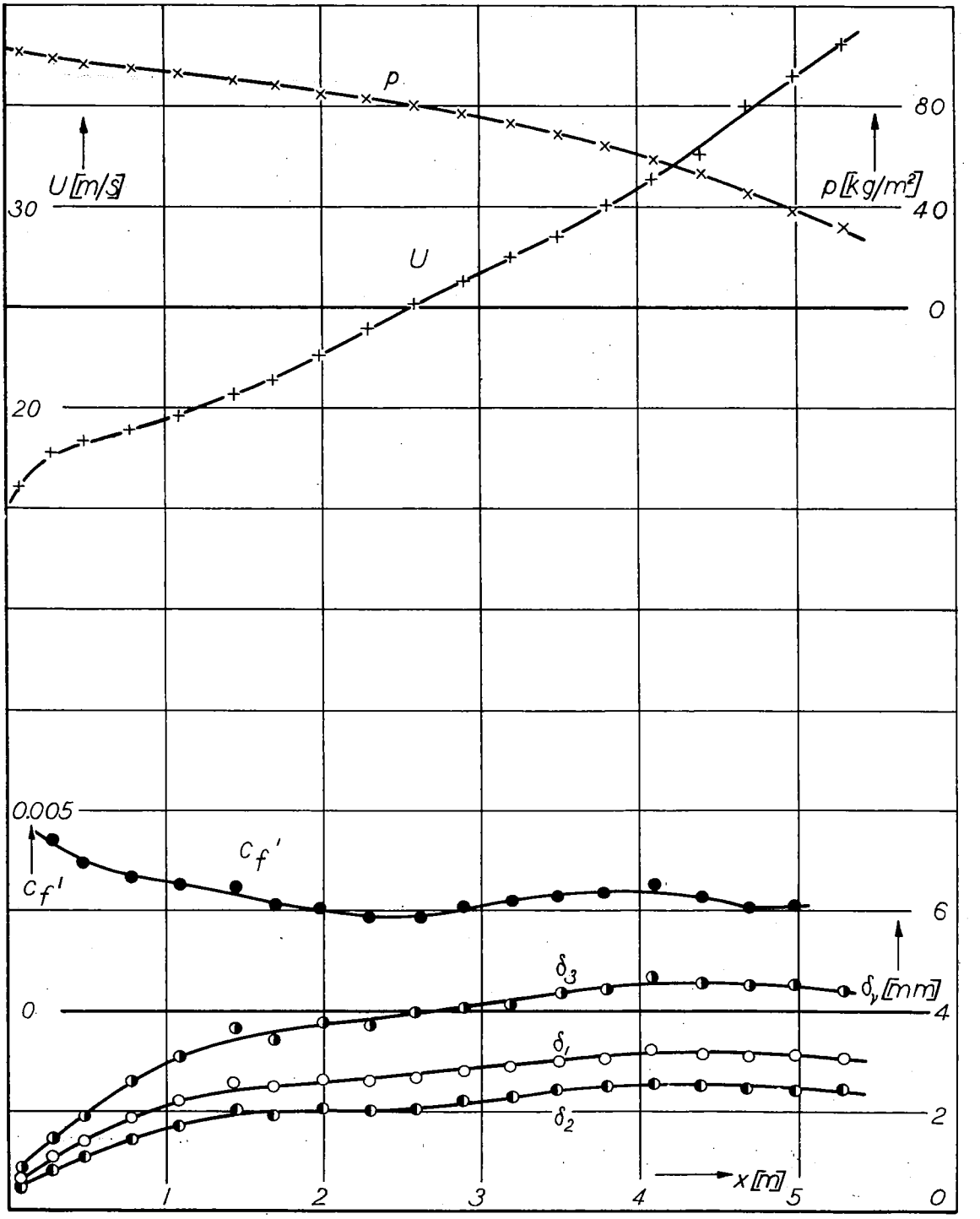

Figure 6.- Pressure drop: Case V. Displacement, momentum, and energy thickness; local drag coefficient.

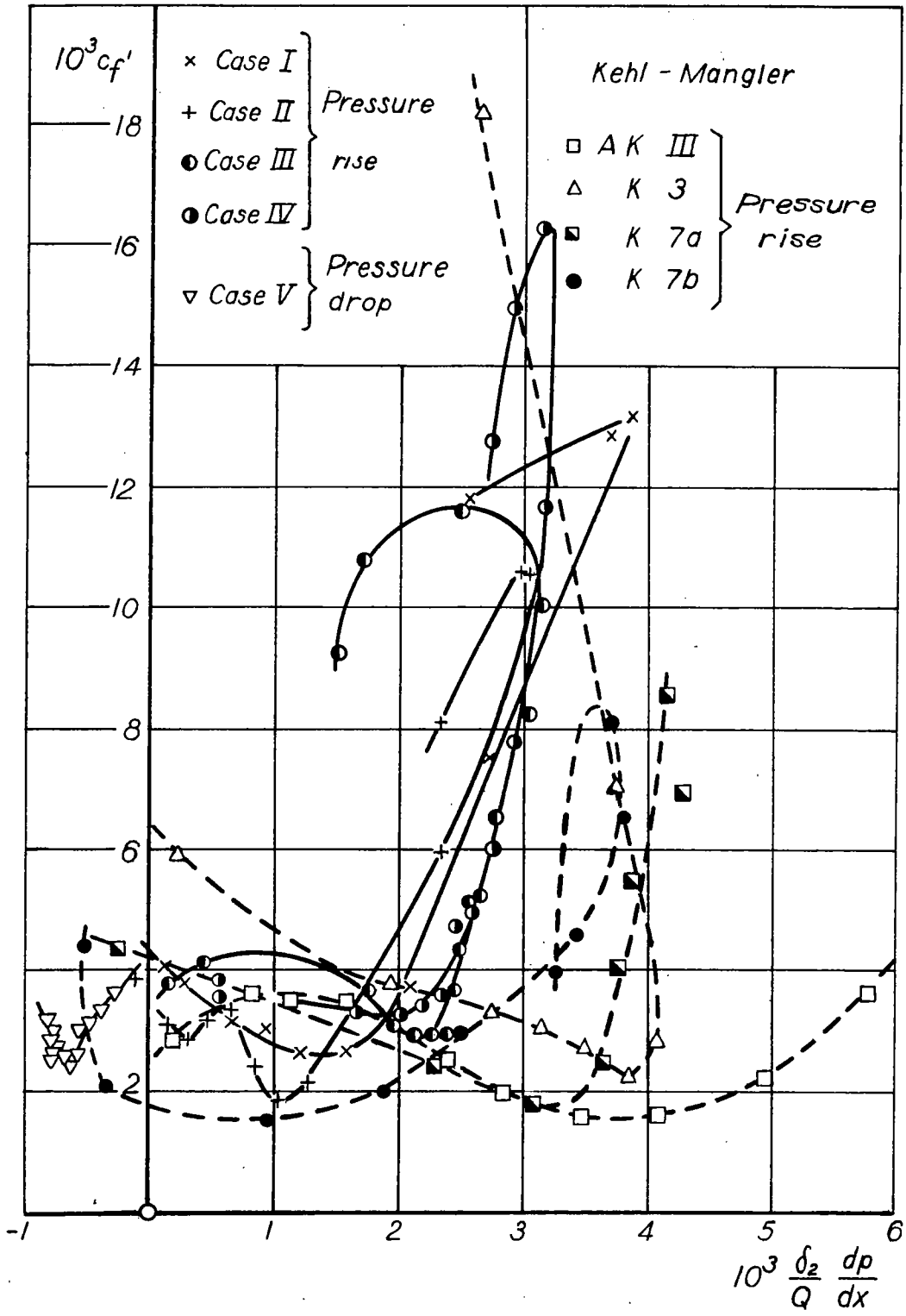

Figure 7.- c_f' against $\frac{\delta_2}{Q} \frac{dp}{dx}$ for pressure rise and pressure drop; comparison with measurements of Kehl.

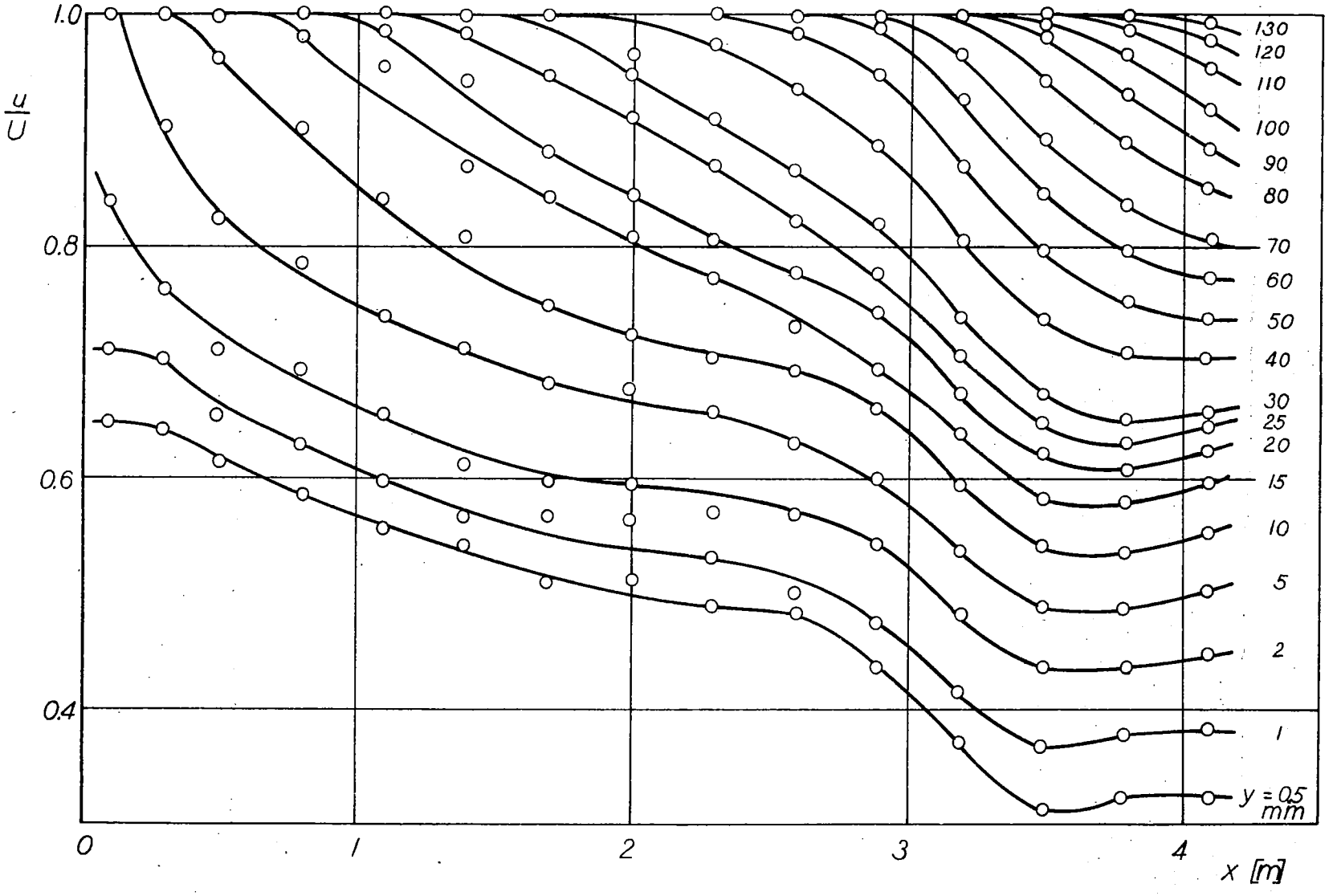

Figure 8.- Velocity distribution at different wall distances for pressure rise, case II.

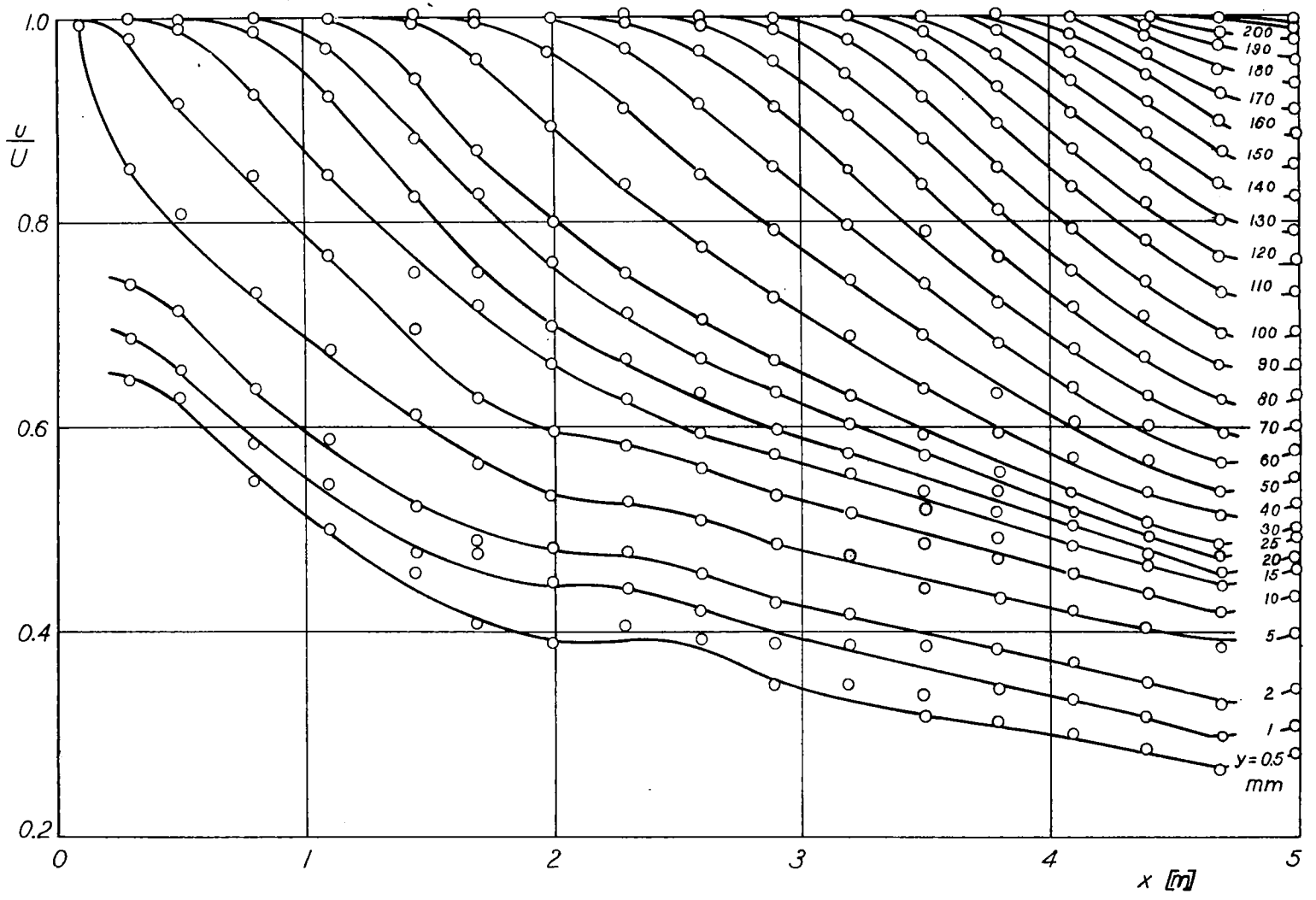

Figure 9.- Velocity distribution at different wall distances for pressure rise, case IV.

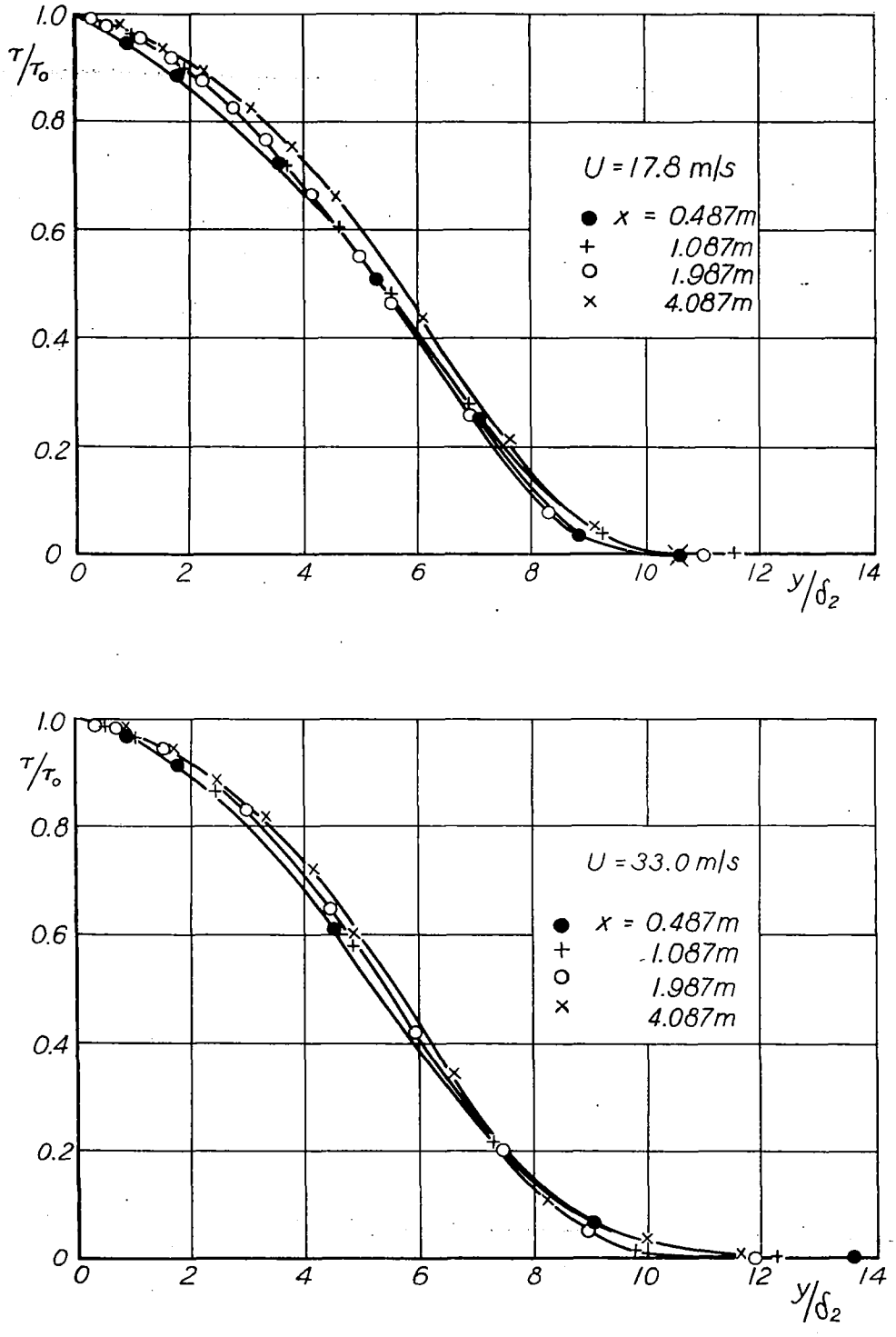

Figure 10.- Dimensionless shearing stress profiles for constant outer velocity.

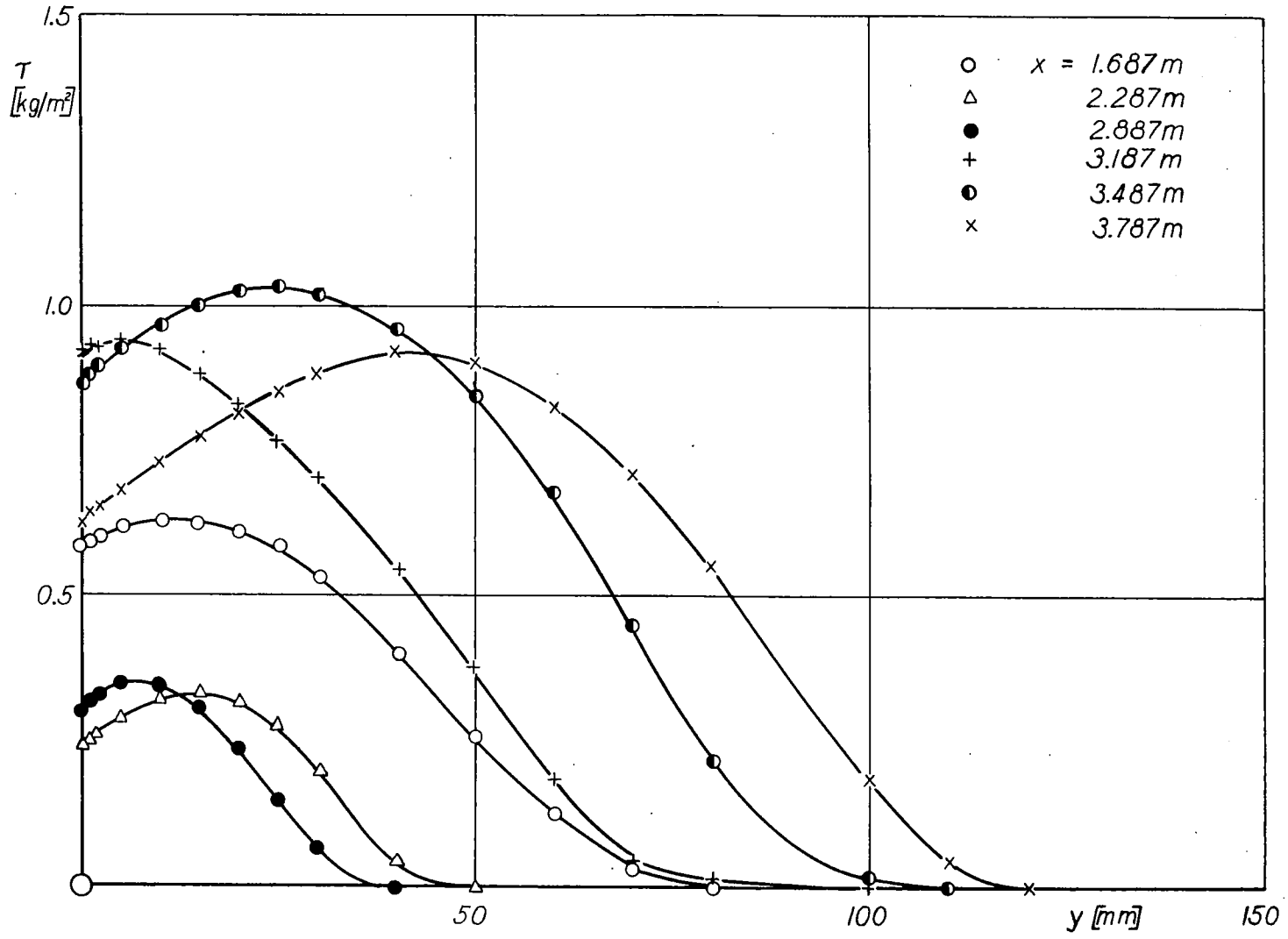

Figure 11.- Shearing stress profiles for pressure rise, case II.

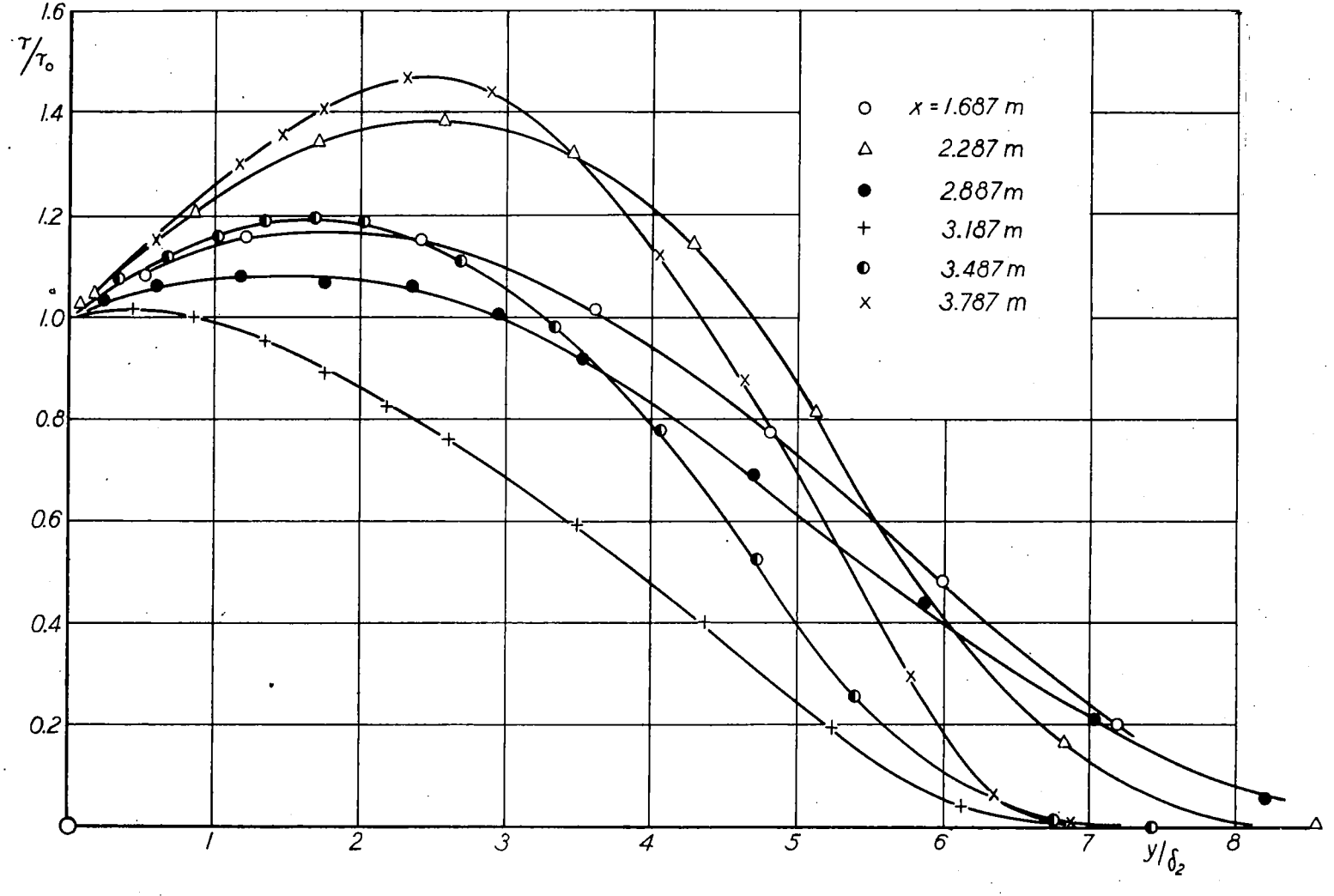

Figure 12.- Dimensionless shearing stress profiles for pressure rise, case II.

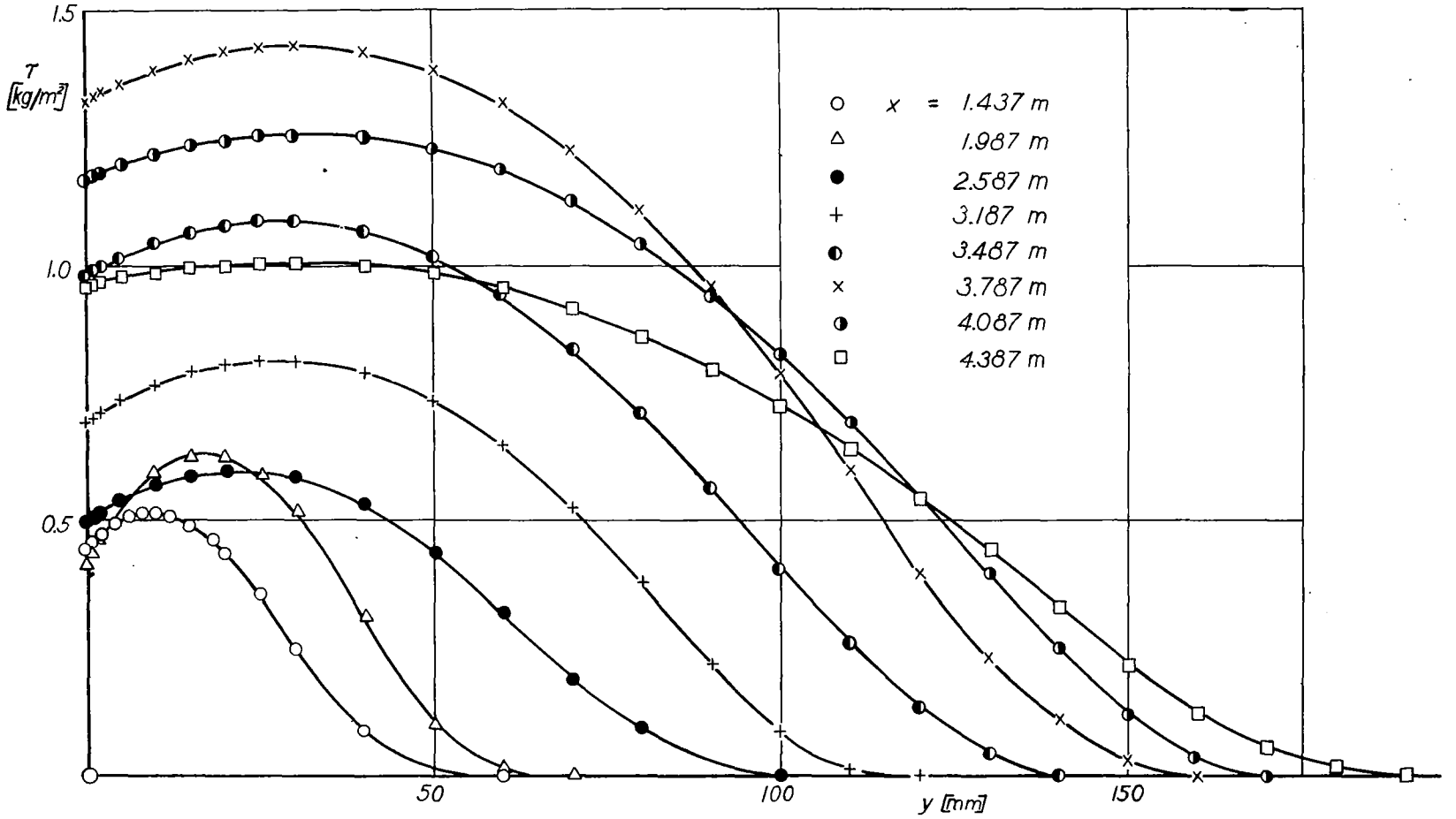

Figure 13.- Shearing stress profiles for pressure rise, case IV.

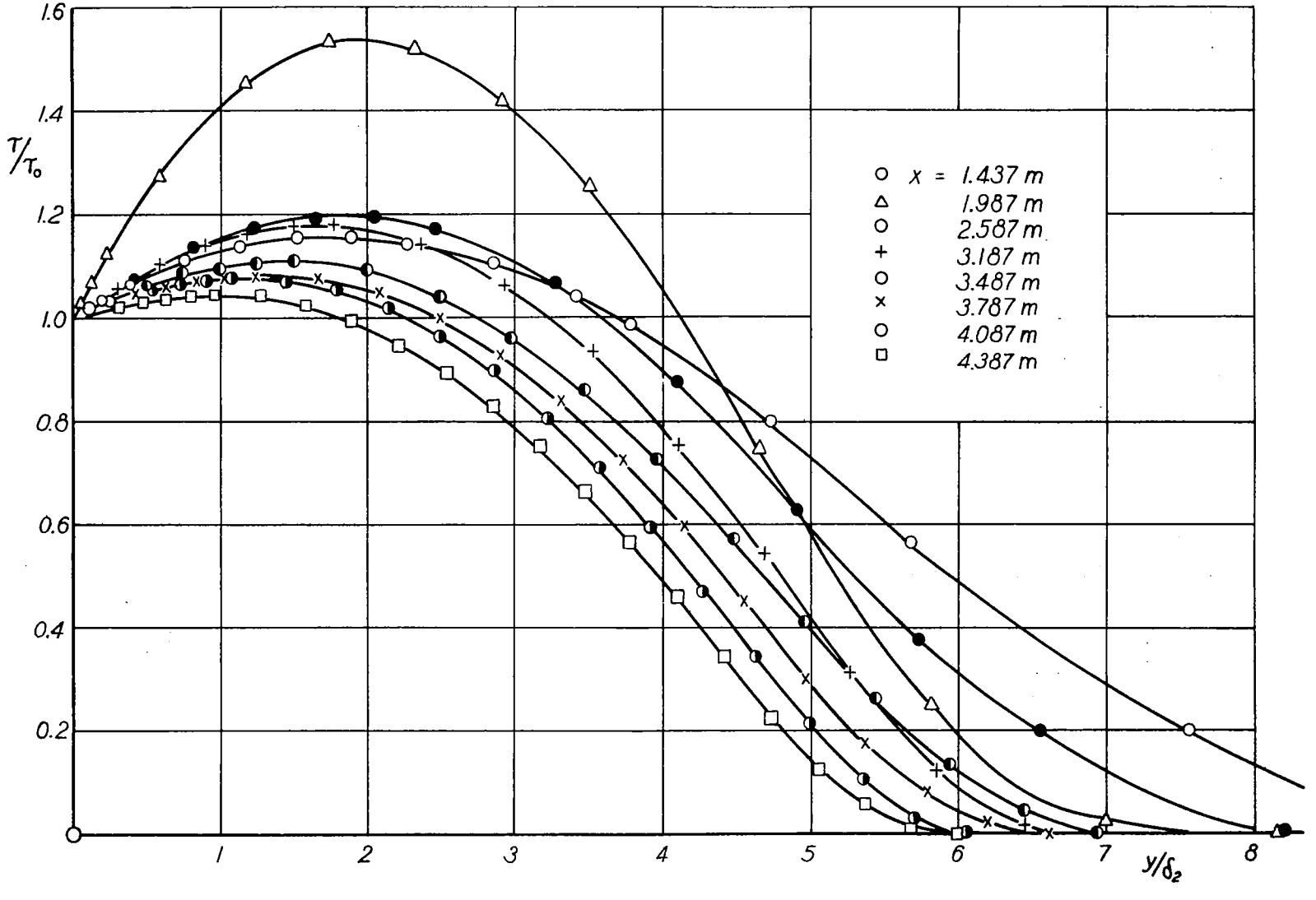

Figure 14.- Dimensionless shearing stress profiles for pressure rise, case IV.

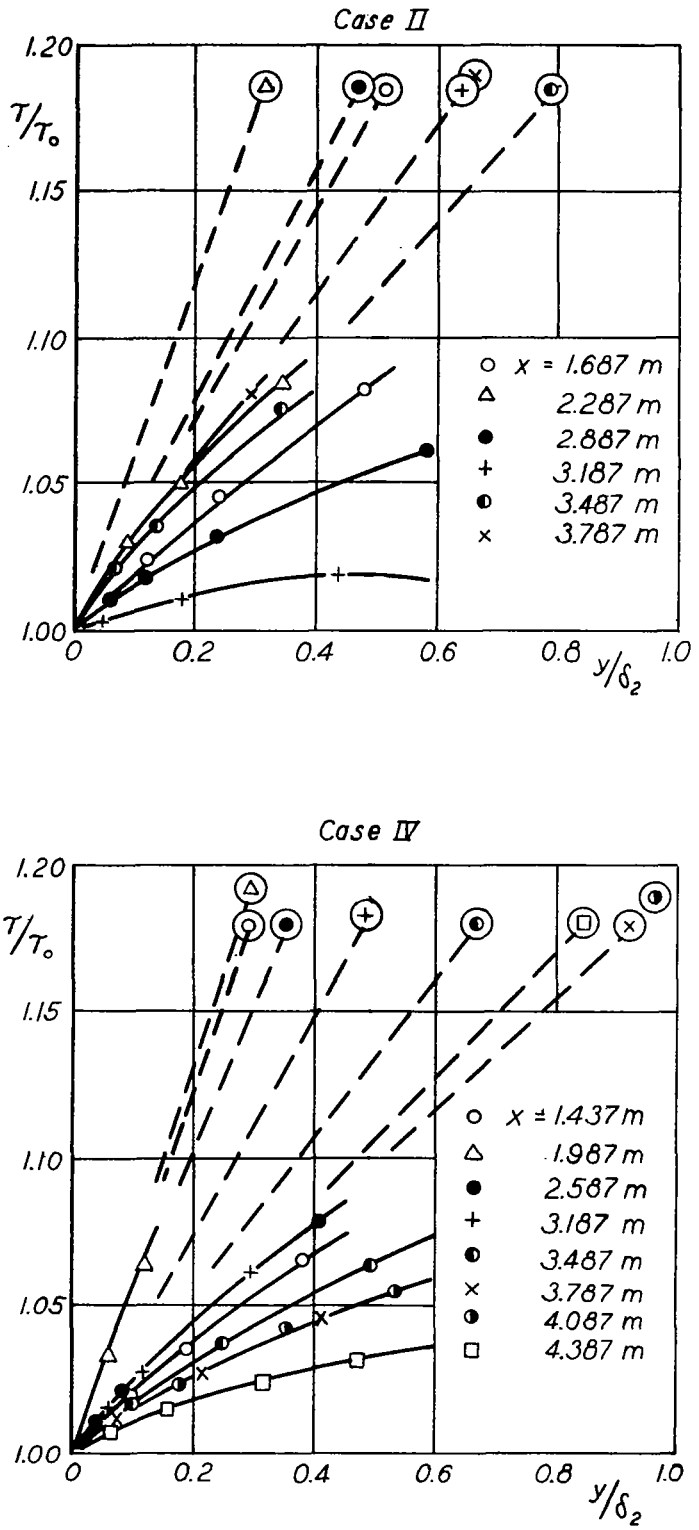

Figure 15.- Shearing stress profiles and wall tangents (Buri form parameter).

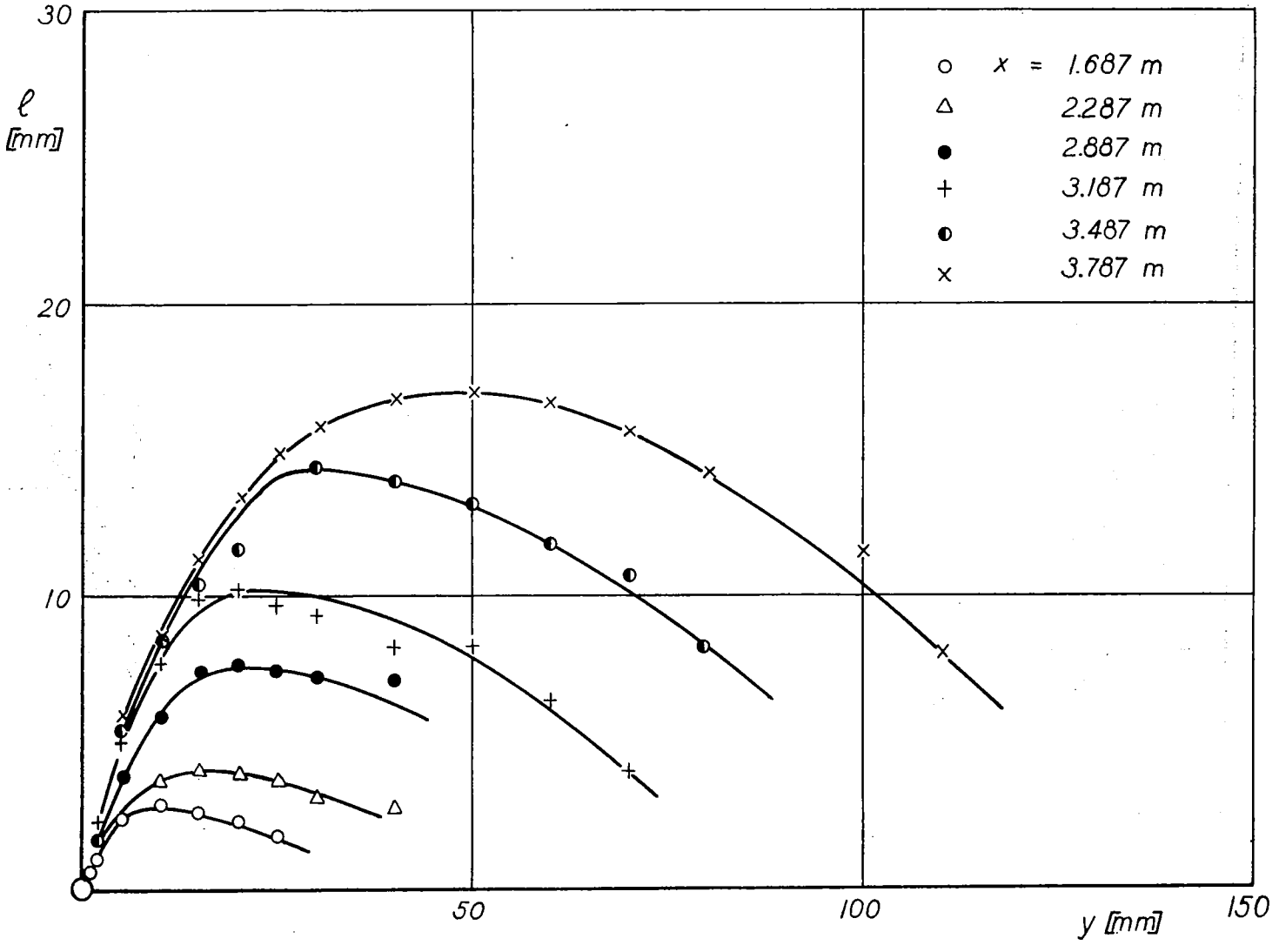

Figure 16.- Mixing length profiles for pressure rise, case II.

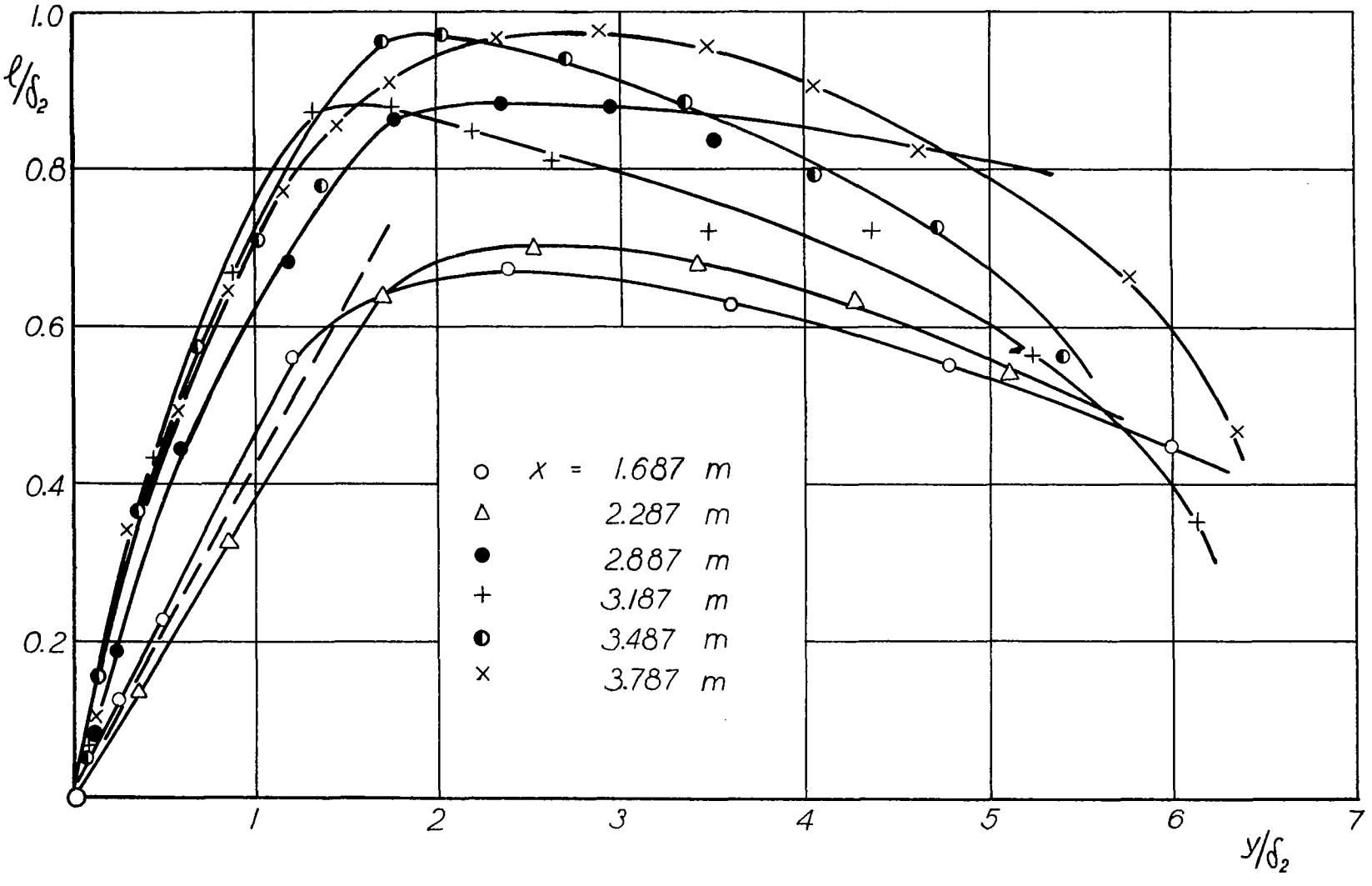

Figure 17.- Dimensionless mixing length profiles for pressure rise, case II.

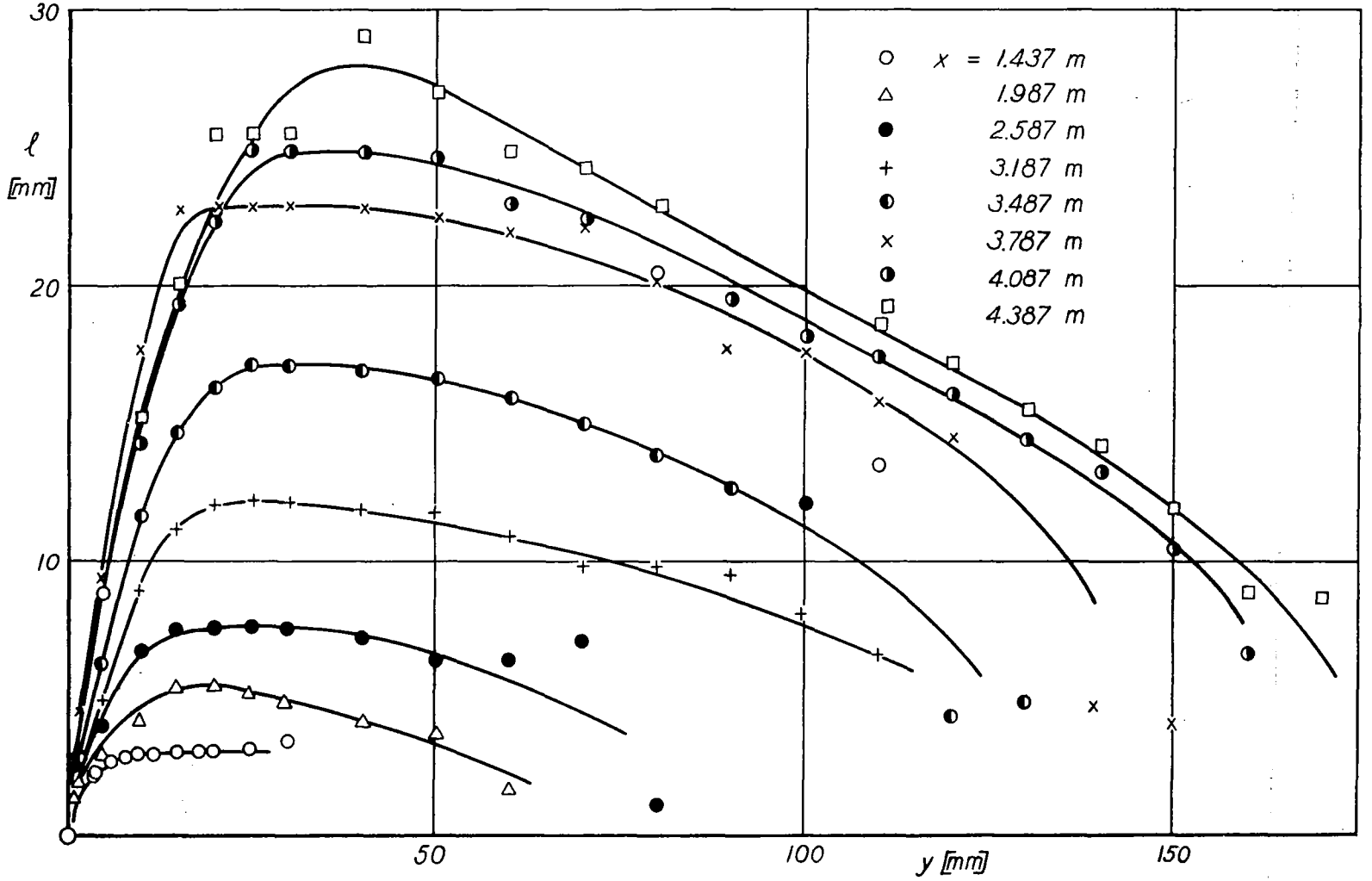

Figure 18.- Mixing length profiles for pressure rise, case IV.

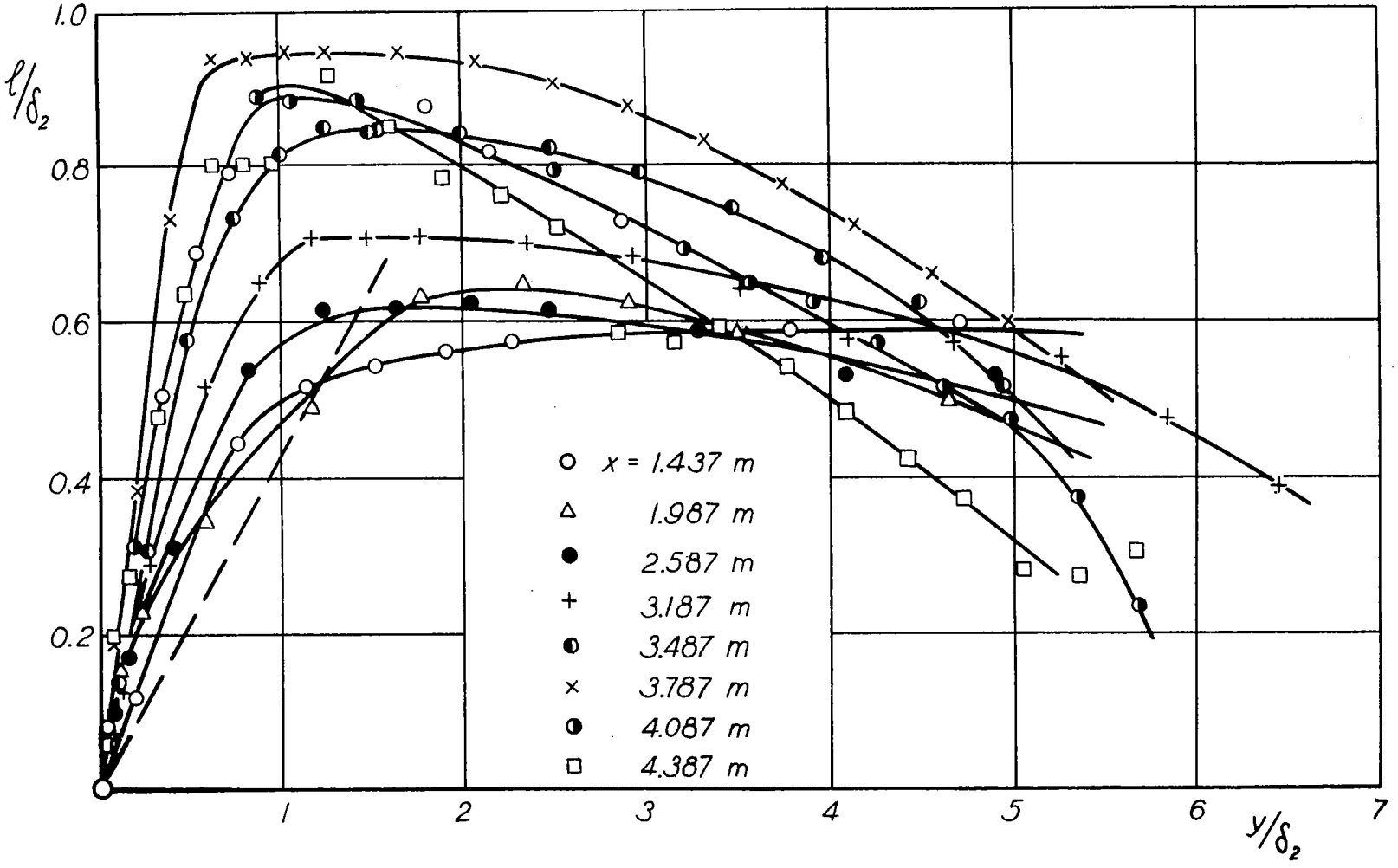

Figure 19.- Dimensionless mixing length profiles for pressure rise, case IV.

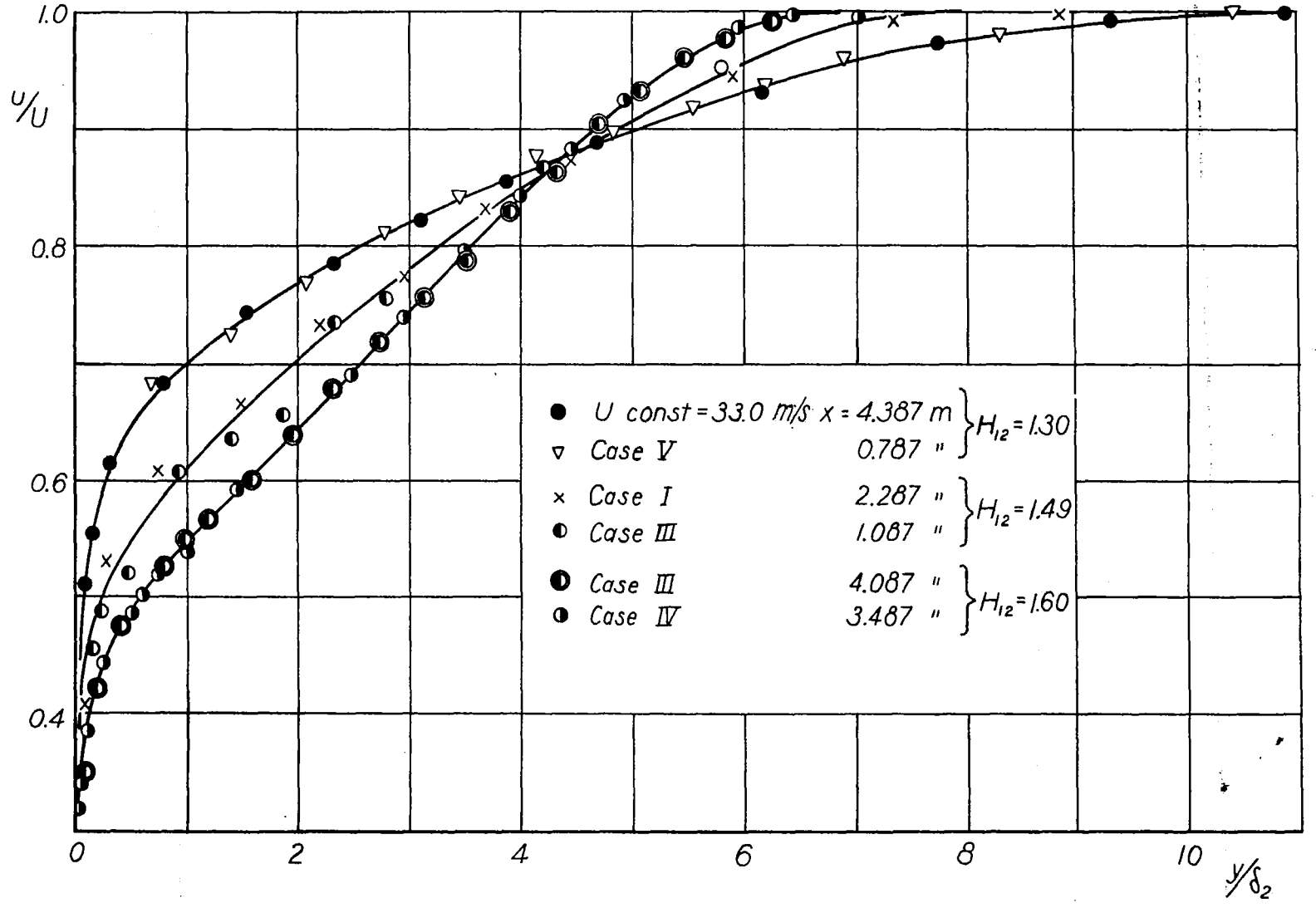

Figure 20.- Dimensionless velocity profiles for various values of H_{12}.

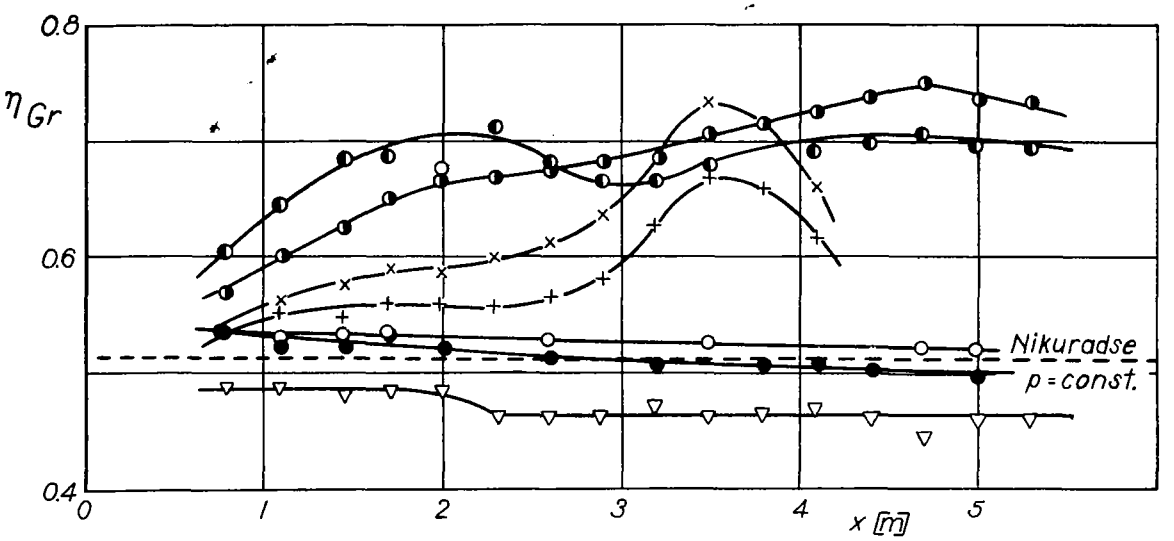

Figure 21.- Variation of η for all measuring series.

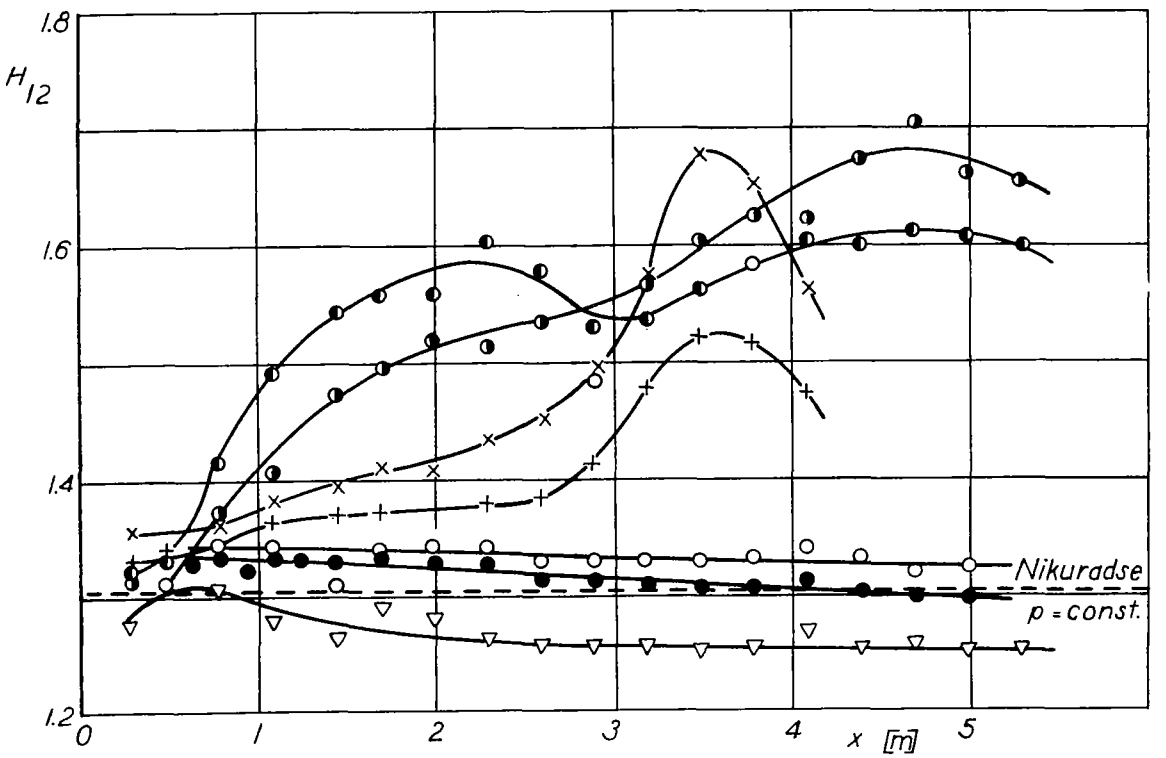

Figure 22.- Variation of H_{12} for all measuring series. (Significance of point markings, compare fig. 23.)

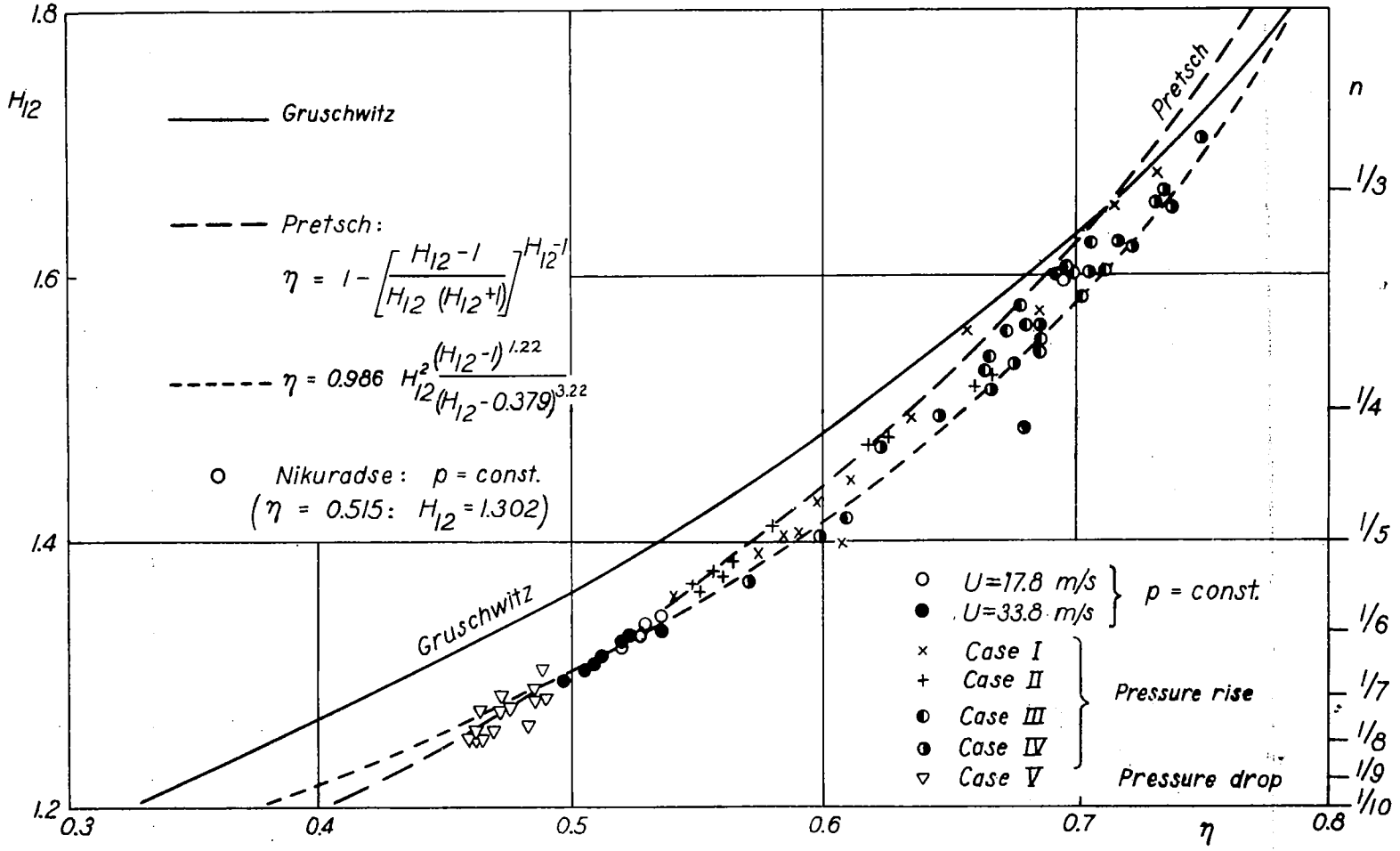

Figure 23.- Relation between H_{12} and η.

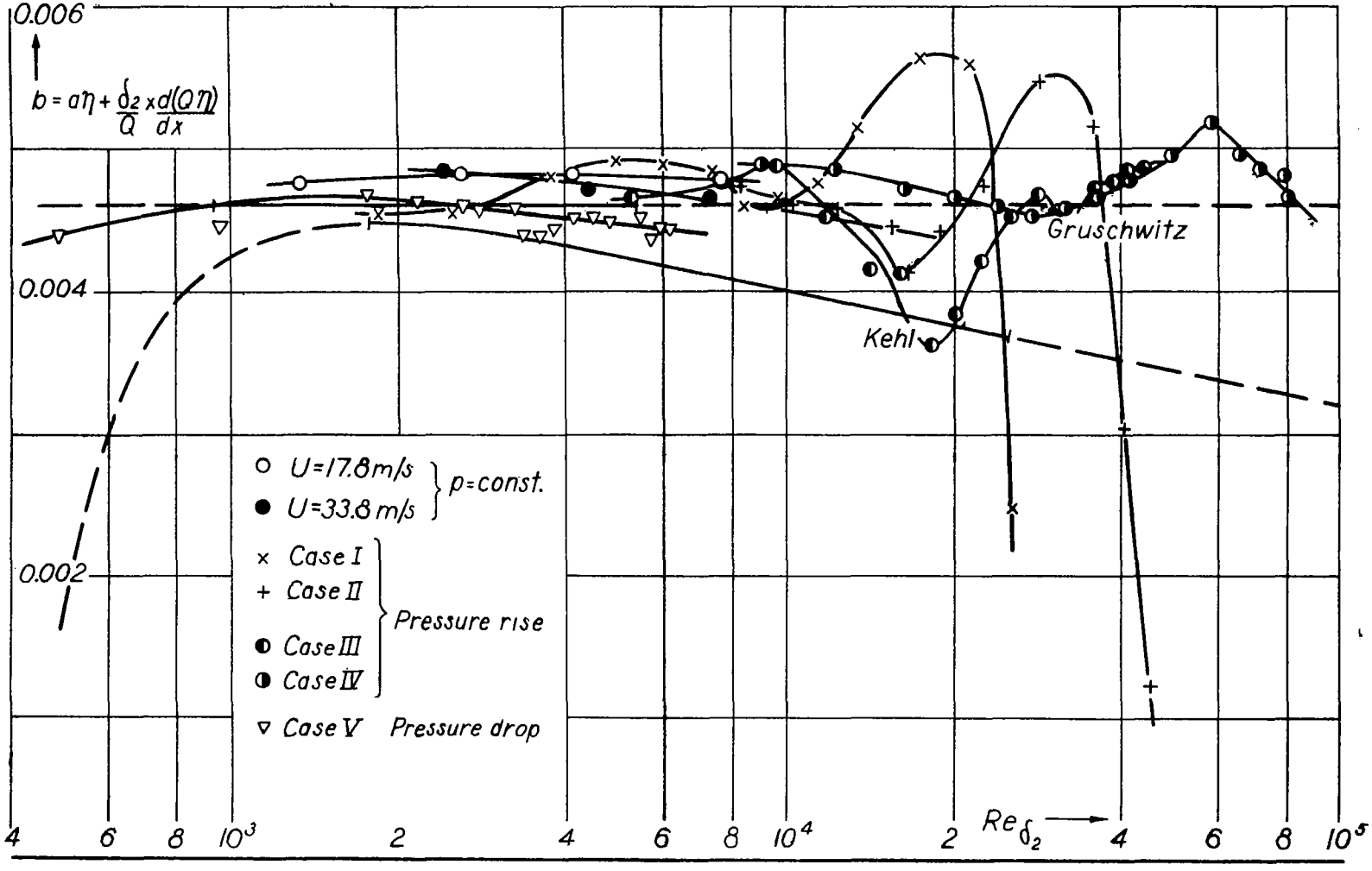

Figure 24.- b as a function of the Reynolds number Re_{δ_2}.

Figure 25.- Measured and calculated variation of δ_2, cases II and IV.

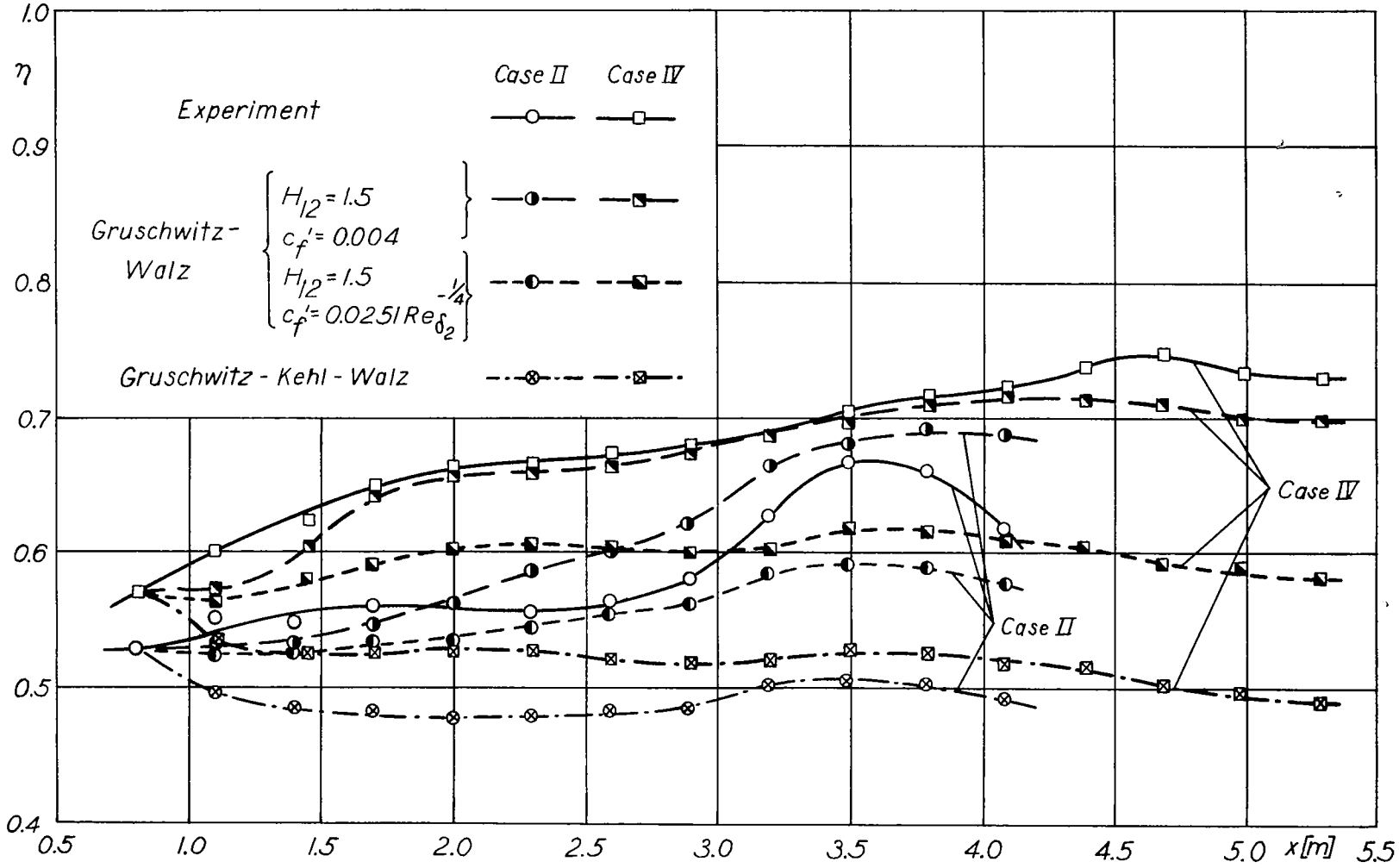

Figure 26.- Measured and calculated variation of η, cases II and IV.

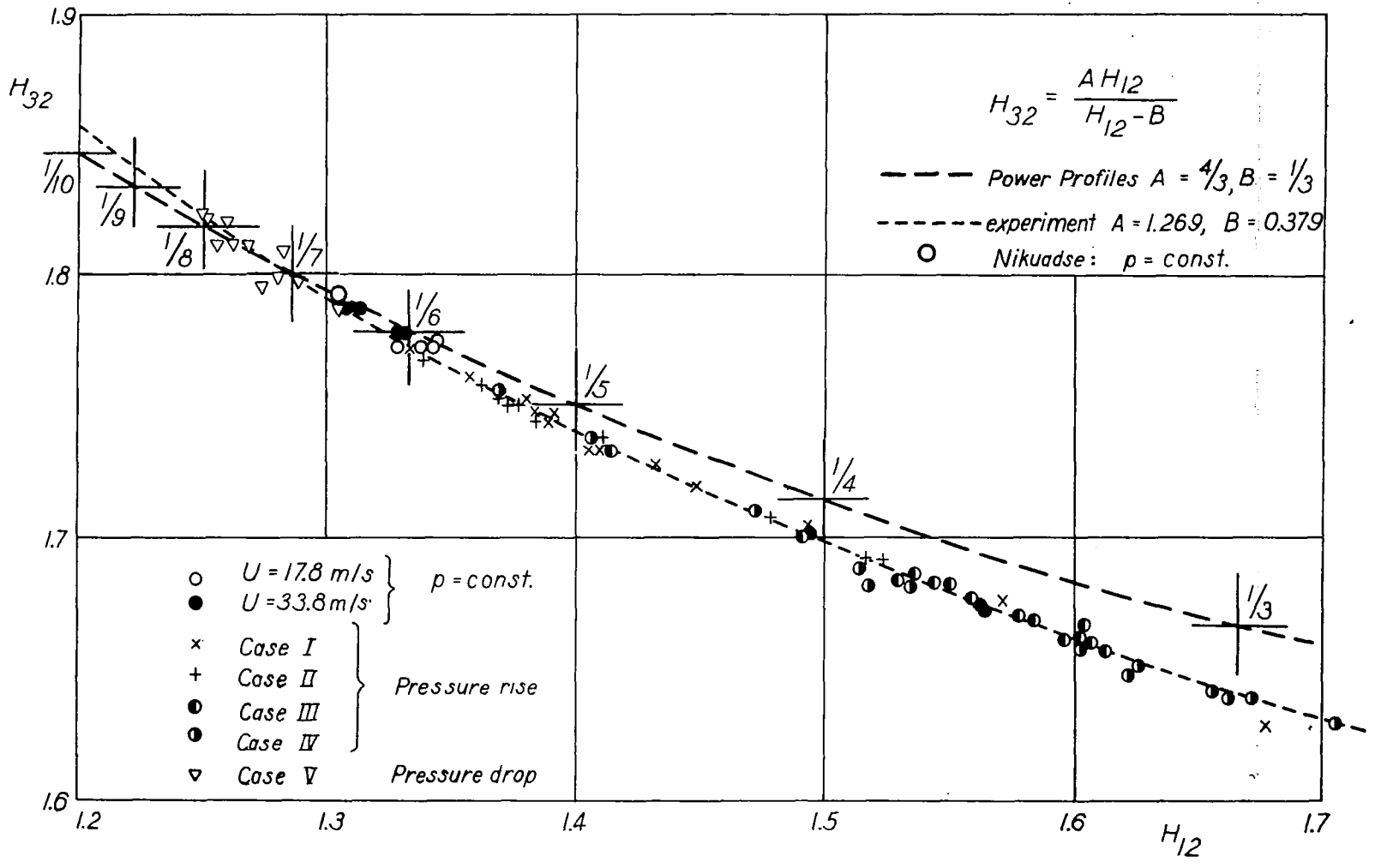

Figure 27.- Relation between H_{32} and H_{12}.

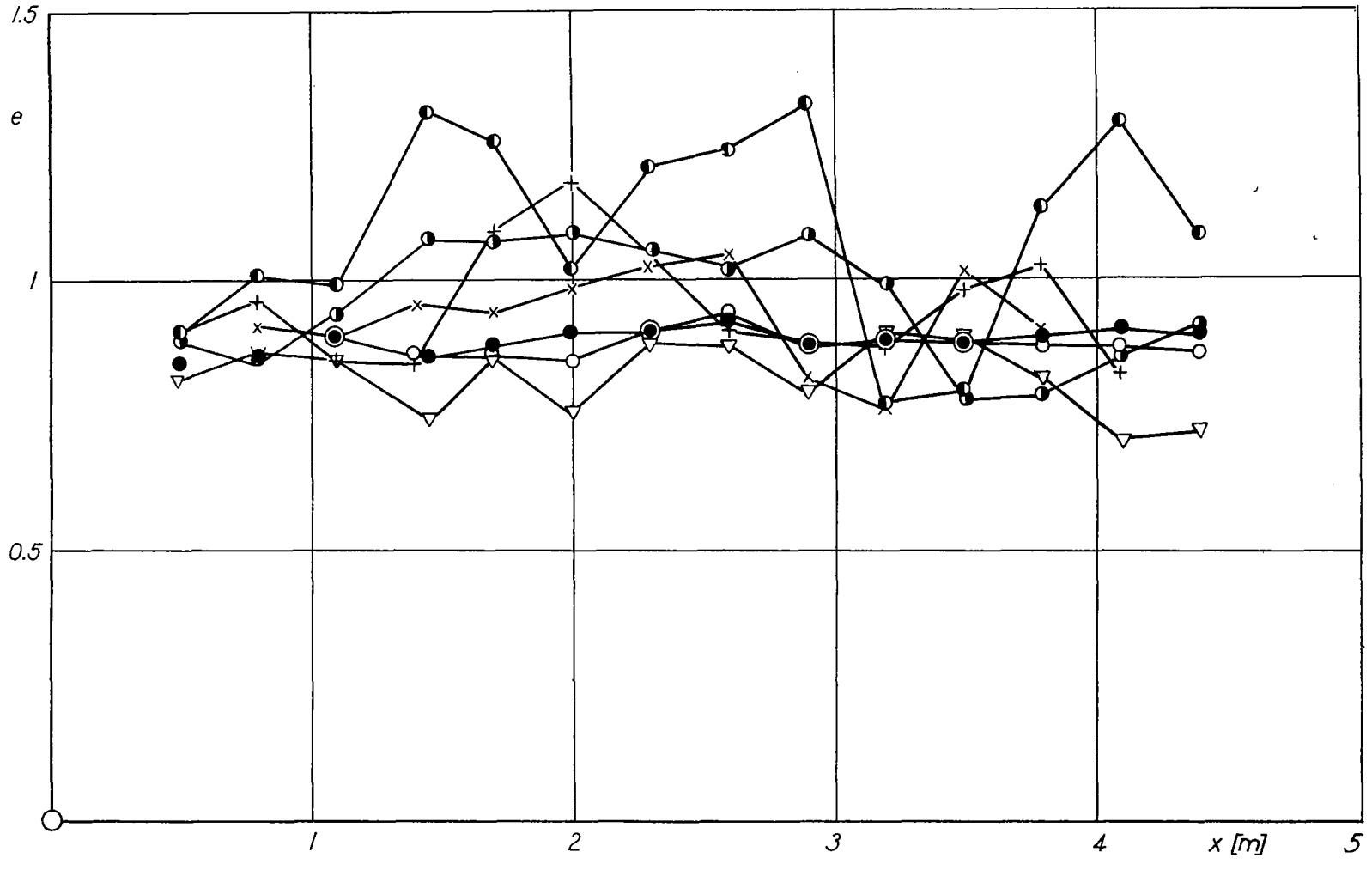

Figure 28.- Variation of e against the rearward position x. (Significance of point markings, compare fig. 27.)

NACA-Langley - 10-4-51 - 1000